The dynamics of diluted bitumen derived oil-mineral aggregates, Part III.

Casey M. O'Laughlin, Brent A. Law, Vanessa S. Zions, Thomas L. King, Brian Robinson, Yongsheng Wu

Science Branch
Fisheries and Oceans Canada
P.O. Box 1006
1 Challenger Drive
Dartmouth NS Canada B2Y4A2

2020

Canadian Technical Report of Fisheries and Aquatic Sciences 3362

Fisheries and Oceans Canada | Pêches et Océans Canada

Canada

Canadian Technical Report of Fisheries and Aquatic Sciences

Technical reports contain scientific and technical information that contributes to existing knowledge but which is not normally appropriate for primary literature. Technical reports are directed primarily toward a worldwide audience and have an international distribution. No restriction is placed on subject matter and the series reflects the broad interests and policies of Fisheries and Oceans Canada, namely, fisheries and aquatic sciences.

Technical reports may be cited as full publications. The correct citation appears above the abstract of each report. Each report is abstracted in the data base *Aquatic Sciences and Fisheries Abstracts*.

Technical reports are produced regionally but are numbered nationally. Requests for individual reports will be filled by the issuing establishment listed on the front cover and title page.

Numbers 1-456 in this series were issued as Technical Reports of the Fisheries Research Board of Canada. Numbers 457-714 were issued as Department of the Environment, Fisheries and Marine Service, Research and Development Directorate Technical Reports. Numbers 715-924 were issued as Department of Fisheries and Environment, Fisheries and Marine Service Technical Reports. The current series name was changed with report number 925.

Rapport technique canadien des sciences halieutiques et aquatiques

Les rapports techniques contiennent des renseignements scientifiques et techniques qui constituent une contribution aux connaissances actuelles, mais qui ne sont pas normalement appropriés pour la publication dans un journal scientifique. Les rapports techniques sont destinés essentiellement à un public international et ils sont distribués à cet échelon. II n'y a aucune restriction quant au sujet; de fait, la série reflète la vaste gamme des intérêts et des politiques de Pêches et Océans Canada, c'est-à-dire les sciences halieutiques et aquatiques.

Les rapports techniques peuvent être cités comme des publications à part entière. Le titre exact figure au-dessus du résumé de chaque rapport. Les rapports techniques sont résumés dans la base de données *Résumés des sciences aquatiques et halieutiques.*

Les rapports techniques sont produits à l'échelon régional, mais numérotés à l'échelon national. Les demandes de rapports seront satisfaites par l'établissement auteur dont le nom figure sur la couverture et la page du titre.

Les numéros 1 à 456 de cette série ont été publiés à titre de Rapports techniques de l'Office des recherches sur les pêcheries du Canada. Les numéros 457 à 714 sont parus à titre de Rapports techniques de la Direction générale de la recherche et du développement, Service des pêches et de la mer, ministère de l'Environnement. Les numéros 715 à 924 ont été publiés à titre de Rapports techniques du Service des pêches et de la mer, ministère des Pêches et de l'Environnement. Le nom actuel de la série a été établi lors de la parution du numéro 925.

Canadian Technical Report of
Fisheries and Aquatic Sciences No. 3362

2020

The dynamics of diluted bitumen derived oil-mineral aggregates, Part III.

by

Casey M. O'Laughlin[1], Brent A. Law[1], Vanessa S. Zions[1], Thomas L. King[2], Brian Robinson[2], Yongsheng Wu[3]

[1] Coastal Ecosystem Science Division
Science Branch
Fisheries and Oceans Canada
P.O. Box 1006
1 Challenger Drive
Dartmouth NS Canada B2Y 4A2

[2] Center for Offshore Oil, Gas & Energy Research
Science Branch
Fisheries and Oceans Canada
P.O. Box 1006
1 Challenger Drive
Dartmouth NS Canada B2Y 4A2

[3] Ecosystem & Ocean Sciences Division
Science Branch
Fisheries and Oceans Canada
P.O. Box 1006
1 Challenger Drive
Dartmouth NS Canada B2Y 4A2

Cat. No. Fs 97-6/3362E-PDF ISBN 978-0-660-34175-1 ISSN 1488-5379

Correct citation for this publication:

O'Laughlin, C., Law, B.A., Zions, V.S., King, T.L., Robinson, B. and Wu, Y. 2020. The dynamics of diluted bitumen derived oil-mineral aggregates, Part III. Can. Tech. Rep. Fish. Aquat. Sci. 3362: vi + 50 p.

TABLE OF CONTENTS

LIST OF TABLES

LIST OF FIGURES

ABSTRACT

O'Laughlin, C., Law, B.A., Zions, V.S., King, T.L., Robinson, B. and Wu, Y. 2020. The dynamics of diluted bitumen derived oil-mineral aggregates, Part III. Can. Tech. Rep. Fish. Aquat. Sci. 3362: vi + 50 p.

The size, settling velocity and bulk density of oil-mineral aggregates represent valuable and sought-after components of predictive oceanographic models designed to forecast the fate of oil spilled in marine and coastal environments. A series of wave tank experiments to analyze the *in situ* formation of oil-mineral aggregates from spilled diluted bitumen have been completed, using a concentration of 50 mg/L^{-1} of fine-grained sediment (median size ~7.5 µm) and chemically dispersed Access Western Blend and Cold Lake Blend diluted bitumen. High-resolution images of settling particles were captured and analyzed for particle size, settling velocity and effective particle density. Tested conditions included colder (< 10°C) and warmer (> 10°C) water with an average salinity of 29.3 ppt. Maximum oil droplet sizes ranged from 750 µm to >1 mm, and the rate of particle clearance from the water column from 0.005 to 0.1 mm·s^{-1}. Results are compared with those of recently published companion reports characterizing previous colder and warmer water, low sediment concentration (15 mg/L^{-1}) experiments. Results are discussed in the context of sediment flocculation and dispersant efficacy.

RÉSUMÉ

O'Laughlin, C., Law, B.A., Zions, V.S., King, T.L., Robinson, B. and Wu, Y. 2020. The dynamics of diluted bitumen derived oil-mineral aggregates, Part III. Can. Tech. Rep. Fish. Aquat. Sci. 3362: vi + 50 p.

La taille, la vitesse de sédimentation et la densité apparente des agrégats pétrole-minéraux sont des éléments précieux et recherchés de modèles océanographiques de prévision conçus pour prévoir le devenir du pétrole déversé dans les environnements marins et côtiers. Une série d'expériences en cuve à houle visant à analyser la formation *in situ* d'agrégats pétrole-minéraux à partir de bitume dilué déversé a été réalisée, en utilisant une concentration de 50 mg/L^{-1} de sédiments à grains fins (taille médiane d'environ 7,5 µm) et de bitume dilué Access Western Blend et Cold Lake Blend dispersé chimiquement. Des images à haute résolution de la sédimentation de particules ont été saisies et analysées pour mesurer la taille des particules, la vitesse de sédimentation et la densité apparente. Les conditions des essais comprenaient une eau plus froide (moins de 10 °C) et plus chaude (plus de 10 °C) avec une salinité moyenne de 29,3 ppm. La taille maximale des gouttelettes d'huile variait de 750 µm à moins de 1 mm, et le taux de séparation des particules de la colonne d'eau de 0,005 à 0,1 mm-s^{-1}. Les résultats sont comparés à ceux des rapports complémentaires récemment publiés qui caractérisent des expériences antérieures sur les eaux plus froides et plus chaudes et les faibles concentrations de sédiments (15 mg/L^{-1}). Les résultats sont discutés dans le contexte de la floculation des sédiments et de l'efficacité des dispersants.

1.0 Introduction

1.1 Initiative

The transport and export of Canadian petroleum products such as diluted bitumen to international markets will elevate the risk of oil spills in marine and coastal environments. The behaviour, transport and fate of non-refined diluted bitumen (dilbit) spilled at sea is not well understood and requires an oceanographic perspective during response to spills. Dilbit is a combination of heavy bitumen oil and lighter diluent, which is added to decrease the viscosity and density of the oil for transport. Predictive models designed to forecast the fate of spilled dilbit require parameters describing the chemical properties and settling dynamics of this material, including its ability to interact with suspended sediment and form oil-mineral aggregates (OMAs). Studies on the transport and fate of OMAs are limited, as are the parameters required to initialize transport models capable of prediction (Gong *et al.*, 2014; Niu *et al.*, 2011). In addition, diluted bitumen has not been extensively considered in previous efforts to determine the behaviour and fate of oil particles in the marine environment, with the exception of recently emerging research (e.g. Yang *et al.*, 2018; Gao *et al.*, 2018; O'Laughlin *et al.*, 2017; Government of Canada, 2013).

1.2 Background

The dynamics, transport and fate of fine-grained sediments in the marine environment is strongly influenced by the process of flocculation, or the tendency of individual suspended particles to amalgamate into larger groups, known as flocs (Kranck and Milligan 1992; Kranck, 1985; McCave, 1984; Kranck, 1973). The increase in size leads flocs to settle faster than their component particles, making floc settling and deposition the main supplier of fine-grained material to the seabed (Curran *et al.*, 2002; Kranck, 1980). A well-flocculated suspension maintains a balance between forces that promote floc growth (e.g. particle contact, adhesion efficiencies) and forces that pull flocs apart (e.g. turbulence, shear forces) (Milligan and Law, 2005; Manning and Dyer, 2002). OMA formation is influenced by a similar balance of parameters, including the concentration of suspended particulate matter (SPM) and the level of mixing energy (Sun *et al.*, 2013; Li *et al.*, 2008; Khelifa *et al.*, 2005). Oil slicks are broken up on the water surface through wave action, tidal mixing or the application of chemical dispersant, forcing oil droplets into the water column where they may interact with micron-scale fine sediment or other suspended particles to form aggregates (Sun and Zheng, 2009; Page *et al.*, 2000; Delvigne, 1987). Two unique forms of OMA, also known as oil-SPM aggregate (OSA) or oil-particle aggregates (OPA), may develop in response to the interaction of oil with suspended particulate (Loh and Yim, 2016; Niu *et al.*, 2016). Firstly, oil droplets can become covered in a sediment coating that reduces their stickiness, preventing droplet re-coalescence and decreasing the adherence of oil to surfaces in the coastal zone (Lee *et al.*, 2003; Page *et al.*, 2000). The sediment coating may also increase oil droplet density, potentially leading to sinking into the water column where biodegradation is most efficient (Venosa and Holder, 2007; Lindstrom and Braddock, 2002). Secondly, another form of OMA may develop as oil-coated particles, occurring where suspended particulate interact with and penetrate the surface of oil droplets (Loh and Yim, 2016).

Most OMA formation occurs at or above a sediment concentration of approximately 50 $mg \cdot L^{-1}$ (Khelifa *et al.*, 2008), although artificial OMA formation has been achieved in concentrations as low as 10 $mg \cdot L^{-1}$ in laboratory settings (Ajijolaiya *et al.*, 2006). Other factors relevant to OMA formation include oil viscosity (Khelifa *et al.*, 2007; 2002), the effects of salinity, water temperature and sediment type (Khelifa *et al.*, 2005; Payne *et al.*, 1989) and other sedimentary properties (Zhang *et al.*, 2010). Other notable effects include the hydrophobicity of minerals (Wang *et al.*, 2013; Wang *et al.*, 2011), the size distribution of oil droplets (Gao *et al.*, 2018) and the interaction of polar compounds in seawater (Khelifa *et al.*, 2002; Stoffyn-Egli and Lee, 2002), which can promote bonds between sediment and oil particles and encourage OMA formation. Chemical dispersants, which are frequently applied as an oil spill countermeasure, have shown a strong influence on OMA formation (Zhang *et al.*, 2010). Dispersants are designed to chemically break down oil slicks by reducing oil-water interfacial tension and producing small oil droplets, accelerating and increasing the overall transfer of oil from the surface into the water column (Li *et al.*, 2008; 2007). The presence of chemical dispersant dominates oil-sediment interactions and overcomes natural oil-sediment sinking dynamics, promoting suspensions of small dispersed oil particles (Lee *et al.* 2008), although many oil particles can re-coalesce and float back to the water surface (Zhang *et al.*, 2010).

Topics including the formation of OMA from diluted bitumen, the behaviour of these aggregate particles and the influence of chemical dispersant on the formation and behaviour of dilbit-derived OMA have not been widely considered. A recent report (Government of Canada, 2013) suggests that dilbit sinks with sufficient mixing in the presence of medium to fined-grained sediment, but also identified knowledge gaps regarding the exact conditions which allow dilbit to sink. It has been shown that dilbit is capable of forming OMA and sinking in freshwater conditions (Lee *et al.*, 2012), and that the chemical composition of various dilbit products has an influence on its fate and behaviour in the marine environment (King *et al.*, 2014). It is desirable to expand this knowledge toward a thorough understanding of the fate and behaviour of dilbit released into the marine environment.

A series of wave tank experiments (WTEs) were designed and completed to investigate the interaction of chemically dispersed dilbit with fine suspended sediment by facilitating *in situ* OMA formation. The goal of this research was to measure changing size, settling velocity and effective density of suspended particles, oil droplets and dilbit-derived OMA, in response to changes in water temperature, sediment concentration, the presence and absence of chemical dispersant, and the particular type of dilbit product. Transport parameters such as the size and settling velocity of dilbit-derived OMA identified by these experiments will contribute to predictive modelling studies designed to forecast the mobility and fate of OMA (e.g. Zhao *et al.*, 2016). Recent work with an idealized oil-particle aggregate model is promising and shows a range of sinking rates linked to dissipation rate, particle grain size and the presence or absence of chemical dispersant (Wu *et al.*, 2016).

2.0 Methodology

Wave tank experiments were completed in the purpose-built wave tank facility (40 m length, 2 m depth, 60 cm width) at the Bedford Institute of Oceanography, in Dartmouth, Nova Scotia, Canada (Figure 1). The wave tank is operated by the Centre for Offshore Oil, Gas and Energy Research, and can accurately simulate the propagation and breaking of deep-water waves, based on linear wave theory (Li *et al.*, 2008; 2007). The computer-controlled wave-generating paddle can produce both regular non-breaking and breaking waves of designated length, height and frequency. For this study, experiments utilized breaking waves with a maximum wave amplitude of 22.5 cm and an average water level in the tank of 1.5 meters (Figure 2). Two previously published companion reports (O'Laughlin *et al.* 2017; 2016) describe and compare results of 15 $mg \cdot L^{-1}$ sediment concentration wave tank experiments, in colder (<10°C) and warmer (>10°C) water conditions. This report, the third in the series, presents results from 50 $mg \cdot L^{-1}$ sediment concentration experiments, which were completed in both colder and warmer water conditions, using two different kinds of chemically-dispersed diluted bitumen (Table 1).

The sediment component used in wave tank experiments was fine-grained material collected from Douglas Channel, British Columbia, Canada. This material was analyzed for disaggregated inorganic grain size using a Coulter Multisizer III electro-resistance particle counter, following methods described by Kranck and Milligan (1985) and Law *et al.* (2013) (Figure 3). Organic components were removed from subsamples of bottom sediment using 35% hydrogen peroxide. Remaining inorganic materials were resuspended in a 1% sodium chloride solution and disaggregated with a sapphire-tipped ultrasonic probe prior to analysis on the Coulter counter. Three aperture tubes (30, 200 and 400 µm) were used to measure particle size, and the results were merged in MATLAB to create continuous grain size spectra, covering a range of 1 to 240 µm. Douglas Channel bottom sediments were generally fine, and predominately composed of fine silts (~40%) and clays (~58%). Sand content was < 3%. Modal and median diameters were 2.6 and 5.0 µm, respectively. Approximately 6 kg of sediment was added to the wave tank to achieve a concentration of ~50 $mg \cdot L^{-1}$ for each experiment.

The chemical dispersant Corexit®EC-9500A was used at a dispersant-to-oil ratio of 1:10. Eight experiments were completed (WTE 21-28), spread over spring and summer months to include potential seasonal variability in particle dynamics and OMA formation, in response to changes in water and air temperature. Water temperatures ranged from 3-8°C during colder water experiments and from 15-18°C during warmer water experiments. Each experiment was divided into three unique 1-hour phases for analysis and comparison: (1) mixing A, with sediment only; (2) mixing B, with sediment, oil and dispersant; and (3), settling. Prior to the start of Mixing A, Bedford Basin seawater was pumped into the wave tank and filtered at 5 µm. Next, sediment was added and waves generated for one hour to produce a homogenous mixture (mixing A). Waves were momentarily shut off for the addition of oil and dispersant to the tank, then restarted to continue mixing for one hour (mixing B). Finally, waves were turned off for the one hour settling phase.

High-resolution images (3296 x 2472 pixels; 93.8 pixels per mm) of suspended and settling particles were collected during experiments using two machine-vision floc cameras (MFVCs) (model Prosilica GX3300 from Allied Vision, 8.0 megapixels). These images were used to produce particle size spectra, covering a range of 45 µm up to several millimeters, and to track the velocity of individual settling particles. The cameras were positioned at different locations in the wave tank to (1) capture both the addition of sediment and dispersed oil, and (2) to observe settling particles at the bottom of the tank (Figure 2). One camera was positioned approximately 10 meters from the wave generating paddle with the sampling zone at 35 cm depth (position B), collecting 1 image every 30 seconds. It was co-located with a Laser in situ scattering and transmissiometry (LISST) instrument, model 100-X (type C), which sampled every 3 seconds over a measurement range of 2.5 to 500 µm. These datasets can be merged to cover a wide range of particle sizes (2.5 µm up to several centimeters). The velocity of settling particles was observed at the distal end of the wave tank (Figure 2) with a further specialized camera, known as the size versus settling machine vision floc camera (SVS-MVFC). This instrument is equipped with a rectangular column (50×10×5 cm) with baffled top above the sampling zone through which settling particles pass. A continuous stream of images were captured by the MVFC-SVS at 11 frames per second, for 30 seconds, at 5 minute intervals. The camera sat at the bottom of the wave tank, approximately 17 meters from the wave generating paddle (position C), with the baffled top at 80 cm depth and the image-collection zone at 130 cm depth. Size versus settling data generated by the SVS-MVFC system include particle size, settling velocity and effective density, defined as the density of particles (e.g. oil, sediment) less the density of seawater (1025 kg/m^3).

Particle size and size-versus-settling relationships were derived from images through analysis completed in MATLAB. Raw image files were converted to greyscale images, and thresholded using Fiji (formerly ImageJ, Schneider *et al.*, 2012). Greyscale threshold values can be used to differentiate particles from the background, and were defined using the triangle method for MVFC images and Otsu's method for SVS-MVFC images (Mikkelsen *et al.*, 2007; Fox *et al.*, 2004). Grain size statistics (particle area, shape descriptors, diameter and perimeter) were calculated, and particle sizes derived from MFVC images were binned to compliment LISST data. Particle size data generated from MFVC images (>45 µm) were manually merged with that of the LISST (2.5 – 500 µm), so as to incorporate the lower end of the size range (2.5 - 45 µm) not captured by the MVFC. Merging of LISST and MVFC data began at the 63 µm bin, where the median bin value is 63.115 µm, to achieve a gradual merge of the two datasets over nine size bins. The resultant value in the 63 µm bin in the merged dataset is derived from 50% LISST data and 50% MFVC data; from here the ratio of contributions from each dataset was changed in 10% increments per bin (e.g. 60%-40%, 70%-30%, etc.), in favor of the dataset with the appropriate size range – the LISST for data covering particle sizes <63 µm, and the MVFC for >63 µm. These data are herein referred to as merged particle size spectra, are plotted as the log of particle diameter (µm) versus the log of volume concentration (ppm) or the log of equivalent weight (%), and cover a range of particle sizes from 2.5 µm to centimeter-scale. Size-settling velocity relationships and effective density estimates were developed from images collected with the SVS-MVFC. Four frames, each separated by one second in time, were overlain to produce a single composite image, which was used to derive continuous tracks for individual particles across the image collection zone. Particles from each frame were numbered and color-coded in composite

images, allowing individual particles to be manually tracked (Mikkelsen *et al.*, 2004). Settling velocity was then calculated, using the distance particles' travel and the time between images. Stagnant particles were deleted during the MATLAB routine prior to settling velocity calculations. In addition, the effective density of settling aggregates was estimated using an inverted Stoke's law method (Fox *et al.*, 2004; Curran *et al.*, 2004).

A handheld YSI system (model 30M) was used to measure water temperature (°C) and salinity (ppt) in wave tank water at the beginning of each experiment. The distribution of suspended materials in the tank was monitored via water samples drawn from multiple locations (Figure 2). In the early stages of experiments, samples were collected from three depths (5, 75 and 145 cm), at three locations (positions A, B and D) every 15 – 20 minutes. Samples were drawn at only one depth at position B (35 cm), to co-locate with the MVFC. Sampling intensity was increased at position D during settling phases while sampling at positions A and B was reduced, in order to mitigate the number of samples and best capture particle-laden water as it moved down the tank. This sampling scheme produced ~70 water samples per experiment. Water samples were vacuum-filtered onto pre-washed, pre-weighed Millipore 8.0 µm cellulose filters, using standard gravimetric methods. Filters were dried at 60°C for 24 hours, then weighed, compared to pre-sample weights and divided by the volume of sample filtered to determine concentration (Law *et al.*, 2008). Water samples collected from the wave tank prior to the addition of sediment were also filtered to characterize the natural background concentration and organic content in Bedford Basin seawater. These filters (Whatman 25 mm glass fiber) were pre-washed, combusted at 550°C for 12 hours, and weighed prior to use.

3.0 Results

The background concentration of suspended materials in the wave tank was generally between 0.3 and 2.0 $mg \cdot L^{-1}$ prior to the addition of sediment. Approximately 30 – 50 % of this material was organic matter present in the seawater (Table 1). Physical properties, including weathering (%), viscosity (centistokes) and density (g/mL) of oils used in wave tank experiments appear in Table 2. The first mixing phase was designed to distribute sediment throughout the tank (Figure 4, time steps 2-6). Suspended particulate matter (SPM) concentration derived from water samples drawn from different locations in the wave tank showed that suspended material was evenly distributed by the end of the second mixing phase, one hour after the addition of dispersed oil (Figure 4, time steps 7-12). At position B, SPM concentration at the end of mixing B ranged from 40 – 60 $mg \cdot L^{-1}$; position D showed a similar range of variability at both 5 and 145 cm depth. Following the mixing phases, the settling period (T>12; waves off) was generally characterized by decreasing SPM at all locations in the wave tank.

MVFC images and LISST data were analyzed at 5 and 15-minute increments (T = 0, 5, 15, 30, 45 and 60) throughout each phase to investigate the size distribution of suspended material. Images collected with the MVFC at position B just prior to, at, and immediately following the addition of oil are shown in Figures 5–12. The elapsed time between Mixing A, T=60 and Mixing B, T=0 was approximately 4-5 minutes, as oil and dispersant were applied. The addition of oil and chemical dispersant to the tank typically generated an increased population of particles

≥100 µm in size; merged particle size spectra derived from MVFC images and LISST data show that maximum particle size of suspended material in the wave tank at the onset of mixing B ranged from 600 µm to >1 mm (Figure 13). Particle size spectra characterizing mixing B throughout each experiment are shown in Figures 14-21. These are generally bimodal, with modes between 12-15 µm and 140-250 µm. The first mode maintains shape but shows more variability in concentration in warmer water (Figures 18-21) than colder water (Figures 14-17). In addition, during colder water experiments the coarser end (>100 µm) of size spectra shows a rapid increase and subsequent reduction in particle population (>75 µm) within 15 minutes of the addition of dispersed oil. Conversely, warmer water experiments tended to show a reduction in particles sized ~10-50 µm immediately following the addition of dispersed oil. In all cases, initially high concentrations of large particles (600 µm to >1 mm) rapidly declined, and within five minutes following the addition of oil and dispersant particle size curves closely reflected that of pre-oil conditions (T=60, Figures 14-21).

Merged particle size spectra characterizing the start of the settling phase is shown in Figure 22. In general, settling phases all showed a tendency toward increasing particle size and concentration with time, although this end result was achieved through a variety of responses (Figures 23-30). Some wave tank experiments (e.g. WTE-24, WTE-27) showed steadily increasing membership in size classes >70 µm over the course of settling phases. In contrast, other experiments (e.g. WTE-21, WTE-25) showed limited change in particle sizes until rapid increases in (1) the concentration of particles >100 µm, and (2) maximum particle size occurred within the final 15 minutes of hour-long settling phases. The development of larger particles (≥1mm) was most prevalent during the final stages of settling in two particular warmer experiments (WTE-25, 26). These two experiments also showed the biggest increase in the concentration of particles sized 400-800 µm, in the form of rapid growth during the final 15 minutes of settling. Water temperature was notably highest (18°C) during these two experiments, compared with other warmer water experiments (15.3 & 16.6°C).

The size of suspended oil droplets was estimated through subtraction of particle size spectra representing pre- and post-oil conditions (Figure 31). Data derived from MVFC images were used for this exercise due to the notable change in the population of particles ≥100 µm following the addition of dispersed oil to the tank. Within 1-2 minutes of the oil and dispersant addition to the wave tank, oil droplets were abundant at the MVFC sampling volume (35 cm depth). Droplets have a notably different appearance than other suspended particles - they adopt a well-defined spherical shape and are highly opaque, making them easy to visually identify in MVFC images (Figure 5). In addition, the timing of their appearance (35 cm depth, position B) correlates very well with the application of chemical dispersant, and the presence of oil at this location was confirmed by water samples. During colder water conditions, maximum droplet sizes ranged from approximately 450 µm to 1 mm; these were larger than those which occurred during warmer water conditions, which ranged from approximately 280-750 µm. The finer end (<120 µm) of oil droplet size spectra was mostly similar for all experiments, while droplets larger than 120 µm were notably more common during colder water conditions.

The SVS-MVFC tracked settling particles that reached the bottom of the wave tank (145 cm). Size versus settling analysis was completed on images collected at five minute intervals

during the settling phases of wave tank experiments (Figures 32-35). Results of size-settling analysis of colder water conditions (WTE-21, 22, 23 & 24) showed settling particles that ranged in size from 40 to 340 µm, settling at rates of 0.05 to 1.4 $mm \cdot s^{-1}$. These particles covered a broad range of effective density, ranging from 10 to 600 kg/m^{-3}. Mean values describing particle size (124-149 µm), settling velocity (0.33-0.38 $mm \cdot s^{-1}$) and effective density (66-76 kg/m^{-3}) during each cold water experiment showed notable similarities. Due to maintenance program requirements on the SVS-MVFC, an older model camera was used during warm water experiments, which did not perform well; data generated was of low quality and has on that basis unfortunately been excluded from this report.

4.0 Discussion

Wave tank experiments, with sediment and oil mixing times of 1 hour and settling phases of 1 hour, completed in colder (3-8°C) and warmer water (15-18°C) with suspended sediment concentration of 50 mg L^{-1}, did not allow for the *in situ* formation of OMA. Although oil droplets were observed in the water column, OMA were not identifiable in images of suspended particles collected at two depths (35 and 145 cm). The absence of OMA in water samples collected from each water sampling station, at each depth, at the end of mixing and settling phases was confirmed by microscope. The two hour time scale available for OMA formation may be a restrictive factor in experiments reported here. Work by Hill *et al.* (2002) suggested that formation times for stabilized OMA can be up to 24 hours, and that formation is likely to be fastest with large oil droplets and high sediment concentration (> 200 $mg \cdot L^{-1}$). Previous research using a variety of oil products (Khelifa *et al.*, 2008b; Ajijolaiya *et al.*, 2006; Hill *et al.*, 2002) also suggested that OMA formation would be most efficient with a higher sediment concentration, as well as a longer period for sediment to interact with oil. These results suggest that at a sediment concentration of 50 $mg \cdot L^{-1}$, a formation time of two hours was not sufficient for OMA production. However, subsequent 50 $mg \cdot L^{-1}$ sediment concentration wave tank experiments that are currently in analysis, with an extended settling phase (~22 hours) and in warm water conditions, did allow for successful *in situ* OMA formation (Table 5). In addition, OMA formation was detected during chemically-dispersed brackish water (~15 ppt) experiments, also with a 50 $mg \cdot L^{-1}$ sediment concentration. These data will be presented and discussed in subsequent reporting (O'Laughlin *et al.*, in prep).

Merged particle size spectra derived from MVFC and LISST were generally similar for colder (<10°C) and warmer (>10°C) water conditions during sediment and dispersed oil mixing. The most notable changes in size spectra during experiments took place following the addition of dispersed oil to the tank, where colder water conditions showed a temporary increase in concentration of particles >100 µm (Figures 14-17). This increased concentration diminished within five minutes, suggesting those particles were oil droplets temporarily driven into the water column by waves which then resurfaced. In contrast, warmer water experiments trended towards a minor increase in smaller particles, sized 10 to 50 µm, in response to adding dispersed oil (Figures 18-21). In comparing merged particle size spectra at the beginning of sediment and dispersed oil mixing phases (mixing B) from different experiments, the concentration of particles 10-50 µm showed notable variability amongst warmer water experiments (dashed lines, Figure

13). This was in contrast to the strong similarities in results of colder water experiments amongst this size range, which showed only minor differences (solid lines, Figure 13). This range of responses was most likely influenced by the reduced efficacy of chemical dispersant in colder water (Niu *et al.*, 2016; Sørensen *et al.*, 2013; Li *et al.*, 2010), which can be attributed to the increased viscosity of oil associated with lower temperatures. In warmer water conditions, higher water temperatures appeared to promote the rapid production of large numbers of smaller (<50 µm) oil droplets, indicating high dispersant efficacy. However, any increase in dispersant effectiveness in warmer water was short lived, as dispersion in colder water achieved the same general result over a slightly longer time scale. Within 15 minutes, the particle size spectra following dispersion in colder water was similar to that noted after five minutes in warmer water conditions. These results lend further support to the idea that ambient water temperature can exert a notable and immediate impact on the resulting size spectra of chemically dispersed dilbit droplets through the influence of water temperature on oil viscosity (King *et al.*, 2015; Li *et al.*, 2010; Khelifa *et al.*, 2002). While particle size curves all appear to be predominantly bimodal, it should be stated that artefacts of the merging process may enhance the appearance of a bimodal distribution.

During settling phases, merged particle size spectra at position B showed that a general tendency towards particle growth with time was present in all experiments (Figures 23-30). This was achieved through two general types of responses, where (1) gradual particle growth took place throughout settling phases (e.g. WTE-22, 24 & 27), or (2) rapid increases in the maximum particle size and the concentration of particles ≥400 µm, which occurred within the final 15 minutes of the hour-long settling phases (e.g. WTE-25, 26 & 28). Gradual particle growth that took place over the course of settling phases is best explained by flocculation. Results from previously reported 15 mg·L^{-1} wave tank experiments (O'Laughlin *et al.*, 2016) suggest that the presence of chemical dispersant can inhibit particle growth through flocculation. Results presented here support a potential delay in natural flocculation, but overall these data demonstrate that particle growth through flocculation likely can occur in the presence of chemical dispersant. One of the primary drivers of floc development is the concentration of particles in suspension (Kranck, 1981), an increase in which causes more interparticle collisions and can lead to faster flocculation (Eisma, 1986). It follows that the higher concentration suspension (e.g. 50 mg·L^{-1}) used in experiments reported here is more likely to produce sediment flocs on the basis of concentration alone than a lower concentration suspension (e.g. 15 mg·L^{-1}). This suggests that the noted difference in flocculation dynamics in the presence of dispersant may simply be related to the concentration of suspended particles. However, rapid increases in concentration and maximum particle size that were limited to the final stages of settling phases might suggest the influence of a different forcing mechanism. This could be linked to the interaction between suspended particles and chemical dispersant, where the effects of dispersant may have interfered with 'normal' particle dynamics, e.g. the tendency for fine suspended particles to gradually flocculate and settle.

Chemical dispersants like Corexit®EC-9500A are primarily composed of surfactants that pull oil slicks apart by lowering surface tension, and solvents that dissolve oil droplets, to effectively reduce oil and OMA size distributions (Sørensen et al., 2014; Li et al., 2007; Singer et al., 1996). In cases where less suspended material is present (e.g. 15 mg·L^{-1}), particles may

become fully covered by chemical dispersant, potentially reducing particle 'stickiness' or altering the electrical charge on particle surfaces, which may disrupt flocculation. At higher sediment concentrations (e.g. 50 $mg \cdot L^{-1}$), the likelihood of all particles interacting with (and becoming coated by) dispersant is less, thereby producing a lower percentage of dispersant-affected particles and allowing for more 'normal' floc formation in spite of the presence of chemical dispersant. This may delay flocculation until either the effects of dispersant relax (through consumption of constituents via chemical reactions), or concentration overcomes the effects of chemically-influenced particle coatings or charges. Such dynamics may result in a late burst of flocculation and lead to rapid particle growth, as suggested by data gathered during WTE-25, 26 & 28 (Figures 27, 28 & 30).

Similar relationships describing flocculation rate and ability across changing salinities have been identified, where increasing flocculation abilities, efficiencies and rates are associated with increasing salinity; this is most notable in brackish and low-salinity situations (Mietta *et al.*, 2009; van Leussen, 1999), rather with the more saline water used in experiments reported here (27-29 ppt). However, it is not immediately understood why the late burst of floc growth occurred during three of the experiments discussed here – parameters, such as salinity, turbulence, organic content and sediment type, which are thought to be strong influences on the process, remained relatively constant across experiments. Future work may be warranted using dispersant and fine sediment only, to investigate the effects of these chemicals on attractive and repulsive forces on sedimentary particle surfaces, which are known to have impacts on dynamic parameters such as floc rate and efficiency (Eisma, 1986; Kranck, 1981). In addition, consideration of what types of flocs may be formed in the presence of chemical dispersant would also be useful (e.g. compactness, strength). Overall, these results do suggest that in warmer water conditions (>10°C), the dispersion efficacy of Corexit®EC-9500A is greater than that of colder water (<10°C).

Size versus settling relationships derived from images collected with the SVS-MVFC at the bottom (~135 cm depth) of the wave tank show maximum particle sizes ranging from 230-340 µm, settling at velocities of up to 1.3-1.5 $mm \cdot s^{-1}$ (Table 3). These values are comparable with the results of field studies on settling floc dynamics, which described settling velocities on the order of 1.0 $mm \cdot s^{-1}$ (Curran *et al.*, 2007; Hill *et al.*, 2000). The maximum effective density of settling particles ranged from 220-620 $kg \cdot m^{-3}$ (less the density of seawater, 1025 kg/m^3). As mentioned, the older model size versus settling system did not perform well during warm water experiments – image quality was not comparable to that of the modern system, and as a result produced unreliable data. These data (size-settling results from WTE-25, 26, 27 & 28) and derived relationships were excluded from analysis described here.

The effective clearance rate (w_e) is designed to consider the overall rate of removal of particles from the water column, and for the purpose of this study, to evaluate change over a range of water temperatures. The effective, or bulk mean, clearance rate is the settling velocity necessary to explain the rate at which particles are removed from the water column through settling, under the assumption that the water column is well-mixed. This is expressed as:

$$C(t) = C_0 e^{-(w_e/h)t},$$

where C(t) is the observed concentration ($g \cdot l^{-1}$) at time t (s), C_0 is the concentration ($g \cdot l^{-1}$) at time t=0, w_e is the effective clearance rate ($m \cdot s^{-1}$), and h is the SPM sample depth (m) (Curran *et al.,* 2004). Clearance rates reported here were developed from SPM values from water samples drawn from the wave tank at 5 cm depth at position D. While clearance rates on the order of 0.1 $mm \cdot s^{-1}$ have been reported for high concentrations of flocculated fine sediment in the marine environment (e.g. Curran *et al.,* 2004, 2002; Hill *et al.*, 2000), clearance rates in the wave tank were generally low, ranging from 0.005 to 0.1 $mm \cdot s^{-1}$ (Figure 21). The relationship between clearance rate and ambient water temperature for 2015 wave tank experiments can be seen in Figure 36.

To better investigate dispersant efficacy, or the effectiveness of each dispersant application, entropy analysis of raw greyscale images was used to identify differences in particle size distribution characteristics following the application of chemical dispersant. Entropy analysis has previously been applied to evaluate dispersant efficacy (Li *et al.*, 2011), and was completed using a semi-automated MATLAB code (Mikkelsen *et al.*, 2007a). Entropy can be understood as a measure of disorder within a macroscopic system (Journel and Deutsch, 1993), and was used here to compare the shape of particle size distributions to determine the overall effectiveness of each dispersant application. Histograms of greyscale values showed that dispersant efficacy at T=120 (immediately following the addition of dispersed oil) was generally similar in experiments discussed here (Figure 37) and did not provide much insight.

Calculations of dynamic dispersion effectiveness (DDE), which is used to determine the amount of oil (%) that is dispersed into the water column, were applied at two points during each experiment (T=120 min and T=180 min) (Table 5). Dynamic dispersion effectiveness is expressed as:

$$DDE(\%) = \frac{\bar{C}_{effluent}\, Q_{effluent}\, T + \bar{C}_{sample} V_{wt}}{\rho_{oil}\, V_{oil}}\, x\, 100,$$

where $\bar{C}_{effluent}$ is the time-averaged oil concentration in the effluent carried out of the wave tank ($g \cdot L^{-1}$); $Q_{effluent}$ is the flow rate of the current ($L \cdot min^{-1}$); V_{wt} is the total volume of water in the tank (27,000 L); T is the settling duration (60 min); $\bar{C}_{sample}$ is the average concentration of oil remaining in the wave tank after T; ρ_{oil} is the density of the test oil ($g \cdot L^{-1}$); and V_{oil} is the volume of oil used in each experiment (230 - 250 ml) (Li *et al.*, 2010). Results show that DDE is notably higher in water warmer than 10°C (Table 5). These results also show decreasing DDE toward the end of all experiments, likely due to oil droplets resurfacing during the settling phase or heavier oil flocs settling to the bottom of the tank. A poor dispersant application due to high wind conditions corresponds with the least effective dispersion, such as during WTE-24. In such instances, weathering of oil on the water surface would increase viscosity, making the oil less susceptible to natural dissolution through either chemical or physical dispersion. In other cases, applications were notably less affected by wind, and the effectiveness of the actual dispersant application is less likely to be a significant factor in resulting total dispersant efficacy.

5.0 Conclusion

The series of experiments discussed in this report confirm further that ambient water temperature influences the size spectra of chemically dispersed dilbit. In addition, results suggest that the presence of chemical dispersants (e.g. Corexit®EC-9500A) may affect the flocculation efficiency of fine suspended material. Further work on these influences, as well as that of chemical dispersant on attractive and repulsive forces (e.g. organic coatings, electrical charges) that typically bind flocs together, and the nature of the flocs (e.g. compactness, strength) formed in the presence of chemical dispersants, are potential avenues for future consideration. Continuing work in the wave tank includes testing the *in situ* formation of dilbit-derived OMA using extended settling phases and brackish water (~15 ppt), and also using lighter conventional oils. While the limited duration for sediment-oil interaction did not produce OMA during wave tank experiments reported here, successful *in situ* formation of OMA in the wave tank has since been achieved using extended temporal conditions, such as a 22-hour settling period.

Acknowledgements

This research was supported by the Ocean Protection Plan (OPP) and World Class Tanker Safety (WCTS) program, from Fisheries and Oceans Canada. Special thanks to Claire McIntyre and Patrick Toole for wave tank operations, and to Emma Poirier for grain size and image processing.

References

Ajijolaiya, L.O., Hill, P.S., Khelifa, A., Islam, R.M., Lee, K. 2006. Laboratory investigation of the effects of mineral size and concentration on the formation of oil–mineral aggregates. Marine Pollution Bulletin 52: 920–927. http://dx.doi.org/10.1016/j.marpolbul.2005.12.006

Belore, R., Trudel, K., Mullin, J., Guarino, A., 2009. Large-scale cold-water dispersant effectiveness experiments with Alaskan crude oils and Corexit 9500 and 9527 dispersants. Marine Pollution Bulletin 58 (1): 118–128.

Curran, K.J., Hill, P.S., Milligan, T.G. 2002. Fine-grained suspended sediment dynamics in the Eel river flood plume. Continental Shelf Research 22: 2537-2550.

Curran, K.J., Hill, P.S., Milligan, T.G., Mikkelsen, O.A., Law, B.A., Durrieu de Madron, X., Bourrin, F. 2007. Settling velocity, effective density, and mass composition of suspended sediment in a coastal bottom boundary layer, Gulf of Lions, France. Continental Shelf Research 27: 1408–1421. http://dx.doi.org/10.1016/j.csr.2007.01.014

Curran, K.J., Hill, P.S., Schnell, T.M., Milligan, T.G., Piper, D.J.W. 2004. Inferring the mass fraction of floc deposited mud: application to fine-grained turbidites. Sedimentology 51: 927–944. http://dx.doi.org/10.1111/j.1365-3091.2004.00647.x

Delvigne, G. A. L. (1987). Droplet size distribution of naturally dispersed oil. In: Proceedings of the 1987 oil spill conference, Amsterdam, The Netherlands. Pp 29-40.

Eisma, D. 1986. Flocculation and de-flocculation of suspended matter in estuaries. Netherlands Journal of Sea Research 20(2-3): 183–199.

Fox, J.M., Hill, P.S., Milligan, T.G., Boldrin, A. 2004. Flocculation and sedimentation on the Po River Delta. Marine Geology 203: 95–107. http://dx.doi.org/10.1016/S0025-3227(03)00332-3

Gao, Y., Zhao, X., Ju, Z., Yu, Y., Qi, Z., Xiong, D. 2018. Effects of the suspended sediment concentration and oil type on the formation of sunken and suspended oils in the Bohai Sea. Environ. Sci.: Processes Impacts 20: 1404-1413. http://dx.doi.org/10.1039/c8em00293b

Gong, Y., Zhao, X., Cai, Z., O'Reilly, S.E., Hao, X., Zhao, D. 2014. A review of oil, dispersed oil and sediment interactions in the aquatic environment: Influence on the fate, transport and remediation of oil spills. Marine Pllution Bulletin 79: 16–33. http://dx.doi.org/10.1016/j.marpolbul.2013.12.024

Government of Canada. 2013. Federal Government Technical Report: Properties, composition and marine spill behaviour, fate and transport of two diluted bitumen products from the Canadian oil sands. pp. 1–85, ISBN 978-1-100-23004-7 Cat. No.: En84-96/2013E-PDF.

Hill, P.S., Khelifa, A., Lee, K. 2002. Time scale for oil droplet stabilization by mineral particles in turbulent suspensions. Spill Science & Technology Bulletin 8 (1): 73–81. http://dx.doi.org/10.1016/S1353-2561(03)00008-2

Hill, P.S., Milligan, T.G., Geyer, W.R. 2000. Controls on effective settling velocity of suspended sediment in the Eel River flood plume. Continental Shelf Research 20(16): 2095-2111. https://doi.org/10.1016/S0278-4343(00)00064-9

Journel, A.G., Deutsch, C.V. 1993. Entropy and spatial disorder. Mathematical Geology 25 (3): 329-355.

Khelifa, A., Fingas, M., Brown, C. 2008. Effects of Dispersants on Oil-SPM Aggregation and Fate in US Coastal Waters: Final Report Submitted to The Coastal Response Research Center, March 2008, pp. 57.

Khelifa, A., Fieldhouse, B., Wang, Z., Yang, M., Landriault, M., Fingas, C.E., Brown, C.E., Gamble, L. 2007. A Laboratory Study on formation of Oil-SPM aggregates using the NIST standard reference material 1941b, In: Proceeding of the Thirtieth Arctic and marine Oil Spill Program Technical Seminar, Environment Canada, Ottawa, ON: pp. 35–48.

Khelifa, A., Hill, P.S., Lee, K. 2005. Assessment of minimum sediment concentration for OMA formation using a Monte Carlo model, In: Al-Azab, M., El-Shorbagy, W., Al-Ghais, S. (Eds.), Oil Pollution and its Environmental Impact in the Arabian Gulf Region. Elsevier, pp. 93–104. http://dx.doi.org/10.1016/S1571-9197(05)80031-X

Khelifa, A., Stoffyn-Egli, P., Hill, P.S., Lee, K. 2002. Characteristics of oil droplets stabilized by mineral particles: effects of oil type and temperature. Spill Science & Technology Bulletin 8 (1): 19-30.

King, T.L., Robinson, B., Boufadel, M., Lee, K. 2015. Flume tank studies to elucidate the fate and behavior of diluted bitumen spilled at sea. Mar. Pollut. Bull. (2014), http://dx.doi.org/10.1016/j.marpolbul.2014.04.042

Kranck, K. 1973. Flocculation of suspended Sediment in the Sea. Nature 246: 348-350. http://dx.doi.org/10.1038/246348a0

Kranck, K. 1980. Experiments on the significance of flocculation in the settling of fine-grained sediment in still water. Can. J. Earth Sci.17: 1517–1526. http://dx.doi.org/10.1139/e80-159

Kranck, K., Milligan, T.G. 1992. Characteristics of suspended particles at an 11 hour anchor station in San Francisco Bay, California. Journal of Geophysical Research 97 (C7): 11,373–11,382.

Kranck, K., Milligan, T.G. 1985. Origin of Grain Size Spectra of Suspension Deposited Sediment. Geo-Marine Letters 5: 61-66.

Law, B.A., Hill, P.S., Milligan, T.G., Curran, K.J., Wiberg, P.L., & Wheatcroft, R.A. 2008. Size sorting of fine-grained sediments during erosion: results from the western Gulf of Lions. Continental Shelf Research, 28(15), 1935-1946. http://dx.doi.org/10.1016/j.csr.2007.11.006

Law, B.A., Milligan, T.G., Hill, P.S., Newgard, J., Wheatcroft, R.A., Wiberg, P.L. 2013. Flocculation on a muddy intertidal flat in Willapa Bay, Washington, Part I: A regional survery of the grain size of surficial sediments. Continental Shelf Research 60S: S136-S144. http://dx.doi.org/10.1016/j.csr.2012.06.007

Lee, K., Bugden, J., Cobanli, S., King, T., McIntyre, C., Robinson, B., Ryan, S., Wohlgeschaffen, G. 2012. UV-Epifluorescence Microscopy Analysis of Sediments Recovered from the Kalamazoo River. US EPA Kalamazoo Administrative Record. Document, 1277.

Lee, K., Stoffyn-Egli, P., Tremblay, G.H., Owens, E.H., Sergy, G.A., Guénette, C.C., Prince, R.C. 2003. Oil–Mineral Aggregate Formation on Oiled Beaches: Natural Attenuation and Sediment Relocation. Spill Science & Technology Bulletin, Vol. 8, (3): 285–296. http://dx.doi.org/10.1016/S1353-2561(03)00042-2

Li, Z., Lee, K., King, T., Niu, H., Boufadel, M.C., Venosa, A.D. 2011. Application of entropy analysis of *in situ* droplet-size spectra in evaluation of chemical dispersion efficacy. Marine Pollution Bulletin 62: 2129-2136. http://dx.doi.org/10.1016/j.marpolbul.2011.07.012

Li, Z., Lee, K., King, T., Boufadel. M.C., Venosa, A.D. 2010. Effects of temperature and wave conditions on chemical dispersion efficacy of heavy fuel oil in an experimental flow-through wave tank. Marine Pollution Bulletin 60: 1550-1559.

Li, Z., Lee, K., King, T., Boufadel, M.C., Venosa, A.D. 2009. Assessment of chemical dispersant effectiveness in a wave tank under regular non-breaking and breaking wave conditions. Marine Pollution Bulletin 56: 903–912. http://dx.doi.org/ doi:10.1016/j.marpolbul.2008.01.031

Li, Z., Kepkay, P., Lee, K., King, T., Boufadel, M.C., Venosa, A.D. 2007. Effects of chemical dispersants and mineral fines on crude oil dispersion in a wave tank under breaking waves. Marine Pollution Bulletin 54: 983–993. http://dx.doi.org/10.1016/j.marpolbul.2007.02.012

Lindstrom, J.E., Braddock, J.F. 2002. Biodegradation of petroleum hydrocarbons at low temperature in the presence of the dispersant Corexit 9500. Marine Poll. Bulletin 44: 739–747. http://dx.doi.org/10.1016/S0025-326X(02)00050-4

Loh, A., Yim, U.H. 2016. A review of the effects of particle types on oil-suspended particulate matter aggregate formation. Ocean Science Journal 51 (4): 535-548. http://dx.doi.org/10.1007/s12601-016-0050-8

Manning, A. J., Dyer, K. R. 2002. A comparison of floc properties observed during neap and spring tidal conditions. Proceedings in Marine Science 5: 233-250. http://dx.doi.org/10.1016/S1568-2692(02)80019-5.

McCave, I. N. 1984. Size spectra and aggregation of suspended particles in the deep ocean. Deep Sea Research Part A. Oceanographic Research Papers 31(4): 329-352. http://dx.doi.org/10.1016/0198-0149(84)90088-8

Mietta, F., Chassagne, C., Winterwerp, J.C., Manning, A.J. 2009. Influence of shear rate, organic matter content, pH and salinity on mud flocculation. Ocean Dynamics 59: 751-763. http://dx.doi.org/ 10.1007/s10236-009-0231-4

Mikkelsen, O.A., Curran, K.J., Hill, P.S., Milligan, T.G. 2007. Entropy analysis of in situ particle size spectra. Estuarine Coastal and Shelf Science 72: 615-625. http://dx.doi.org/10.1016/j.ecss.2006.11.027

Mikkelsen, O.A., Milligan, T.G., Hill, P.S., Moffat, D. 2004. INSSECT—an instrumented platform for investigating floc properties close to the seabed. Limnology and Oceanography Methods 2: 226-236.

Milligan, T. G., & Law, B. A. 2005. The effect of marine aquaculture on fine sediment dynamics in coastal inlets. In: Environmental Effects of Marine Finfish Aquaculture (239-251). Springer Berlin Heidelberg. http://dx.doi.org/10.1007/b136013

Niu, H., Li, Z., K., Lee, K., Kepkay, P., Mullin, J.V. 2011. Modelling the Transport of oil-mineral aggregates (OMAs) in the Marine Environment and Assessment of Their Potential Risks. Environmental Modelling and Assessment 16 (1): 61-75. http://dx.doi.org/10.1007/s10666-010-9228-0

Niu, H., Li, P., Yang, R., Wu, Y., Lee, K. 2016. Effects of chemical dispersant and seasonal conditions on the fate of spilled oil – modelling of a hypothetical spill near Saint John, NB. Water Quality Research Journal of Canada: 51.3. http://dx.doi.org/10.2166/wqrjc.2015.018

O'Laughlin, C., Law, B.A., Zions, V.S., King, T.L., Robinson, B., Wu, Y. 2017. Settling of dilbit-derived oil-mineral aggregates (OMAs) & transport parameters for oil spill modelling. Marine Pollution Bulletin 124(1): 292-302. http://dx.doi.org/10.1016/j.marpolbul.2017.07.042

O'Laughlin, C., Law, B.A., Zions, V.S., King, T.L., Robinson, B., Wu, Y. 2016. The dynamics of diluted bitumen derived oil-mineral aggregates, Part I. Can. Tech. Rep. Fish. Aquat. Sci. No. 3157.

Page, C.A., Bonner, J.S., Sumner, P.L., McDonald, T.J., Autenrieth, R.L., Fuller, C.B. 2000. Behaviour of a chemically dispersed oil and a whole oil on a nearshore environment. Wat. Res. 34 (9): 2507-2516. http://dx.doi.org/10.1016/S0043-1354(99)00398-X

Schneider, C.A., Rasband, W.S., Eliceiri, K.W. 2012. NIH Image to ImageJ: 25 years of image analysis. Nature Methods 9: 671-675.

Sørensen, L., Melbye, A.G., Booth, A.M. 2014. Oil droplet interaction with suspended sediment in the seawater column: Influence of physical parameters and chemical dispersants. Marine Pollution Bulletin 78: 146-152. http://dx.doi.org/10.1016/j.marpolbul.2013.10.049

Sun, J., Zheng, X. 2009. A review of oil-suspended particulate matter aggregation – a natural process of cleansing spilled oil in the aquatic environment. Journal of Environmental Monitoring 11: 1801-1809. http://dx.doi.org/10.1039/b904829b

Sun, J., Zhao, D., Zhao, C., Liu, F., Zheng, X. 2013. Investigation of the kinetics of oil–suspended particulate matter aggregation. Marine Pollution Bulletin 76: 250–257. http://dx.doi.org/10.1016/j.marpolbul.2013.08.030

van Leussen, W. 1999. The variability of settling velocities of suspended fine-grained sediment in the Ems estuary. Journal of Sea Research 41: 109-118. https://doi.org/10.1016/S1385-1101(98)00046-X

Venosa, A.D., Holder, E.L., 2007. Biodegradability of dispersed crude oil at two different temperatures. Marine Pollution Bulletin 54: 545–553. http://dx.doi.org/10.1016/j.marpolbul.2008.01.031

Wang, W., Zhang, Y., Lee, K. 2013. Role of the hydrophobicity of mineral fines in the formation of oil-mineral aggregates. Canadian Journal of Chemical Engineering: 91: 698-703.

Wang, W., Zheng, Y., Li, Z., Lee, K. 2011. PIV investigation of oil- mineral interaction for an oil spill application. Chemical Engineering Journal 170 (1): 241-249. http://dx.doi.org/10.1016/j.cej.2011.03.062

Wu, Y., C.G. Hannah, B. Law, T. King, and B. Robinson. 2016. An Estimate of the Sinking Rate of Spilled Diluted Bitumen in Sediment Laden Coastal Waters. Proceedings of the Thirty-ninth AMOP Technical Seminar, Environment and Climate Change Canada, Ottawa, ON, pp. 331-347, 2016.

Yang, Z., Hua, Y., Mirnaghi, F., Hollebone, B.P., Jackman, P., Brown, C.E., Yang, C., Shah, K., Landriault, M., Chan, B. 2018. Effect of evaporative weathering and oil-sediment interaction on the fate and behaviour of diluted bitumen in marine environments. Part 2. The water accommodated and particle-laden hydrocarbon species and toxicity of the aqueous phase. Chemosphere 191: 145-155.

Zhang, H., Khatibi, M., Zheng, Y., Lee, K., Li, Z., Mullin, J.V. 2010. Investigation of OMA formation and the effect of minerals. Marine Pollution Bulletin 60: 1433–1441. http://dx.doi.org/10.1016/j.marpolbul.2010.05.014

Zhao, L., Boufadel, M.C., Geng, X., Lee, K., King, T., Robinson, B., Fitzpatrick, F. 2016. A-DROP: A predictive model for the formation of oil particle aggregates (OPAs). Marine Pollution Bulletin 106 (1-2): 245-259. http://dx.doi.org/10.1016/j.marpolbul.2016.02.057

Figure 1: *(a) Wave tank facility at Bedford Institute of Oceanography; (b) sediment mixing, before oil is added (dilbit sample in foreground); (c) spilling the oil, and (d) spilled oil within the containment ring, prior to wave action.*

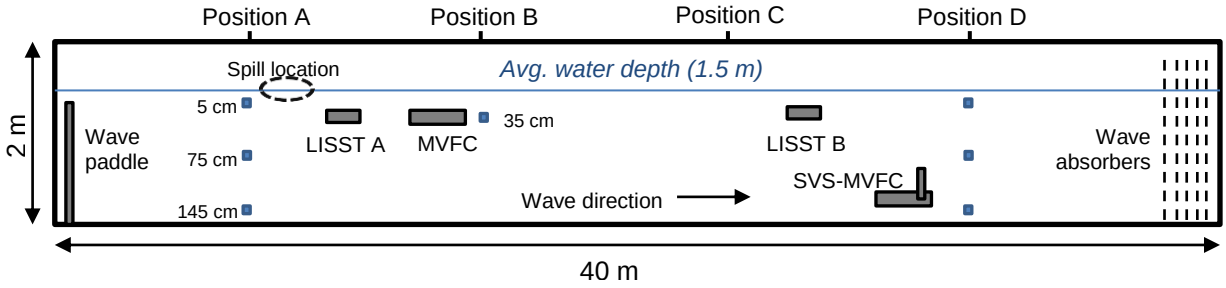

Figure 2: *Schematic diagram of the instrumental set-up used during wave tank experiments.*

Table 1: *Experimental conditions for four colder water (3-8°C) and four warmer water (15-18°C) wave tank experiments, including water temperature (°C), salinity (ppt), and organic content (%), suspended sediment concentration (mg/L), source and amount added to the tank to achieve 50 mg/L concentration, and the type and amount of oil used in each experiment. All experiments were chemically dispersed with Corexit®EC-9500A at a dispersant to oil ratio of 1:10.*

Experiment	Temp.	Salinity	Background		Sediment		Oil	
			SPM	organic				
	(°C)	(ppt)	(mg/L)	(%)	Source	Amount (g)	Type	Amount (g)
WTE-21	3.4	29.5	2.06	45.1	DC-04	6934.0	CLB	261.7
WTE-22	6.5	27.3	4.19	44.0	DC-04	6936.0	CLB	234.1
WTE-23	5.1	28.7	2.41	43.9	DC-04	6937.0	AWB	250.1
WTE-24	8.0	29.6	3.43	30.6	DC-04	6923.0	AWB	226.8
WTE-25	18.0	29.1	3.15	39.6	DC-04	6930.0	CLB	250.0
WTE-26	18.0	29.0	2.67	43.1	DC-04	4373.0	CLB	245.1
WTE-27	15.3	29.2	n/a	n/a	DC-04	4374.0	AWB	247.0
WTE-28	16.6	28.4	3.12	49.0	DC-04	4374.0	AWB	232.3

Table 2: *Physical properties of Cold Lake Blend (CLB) and Access Western Blend (AWB) oils which were used in this study, including the amount of weathering (%), oil viscosity (centistokes) at 15°C and 40°C, and oil density (g/ml) at 15°C and 40°C.*

Dilbit product	% Weathered	Viscosity (centistokes)		Density (g/mL)	
		15°C	40°C	15°C	40°C
Cold Lake Blend (Winter Blend)	6.20%	1293.4	211.7	0.951	0.934
Access Western Blend (Winter Blend)	7.00%	1402.0	227.6	0.948	0.931

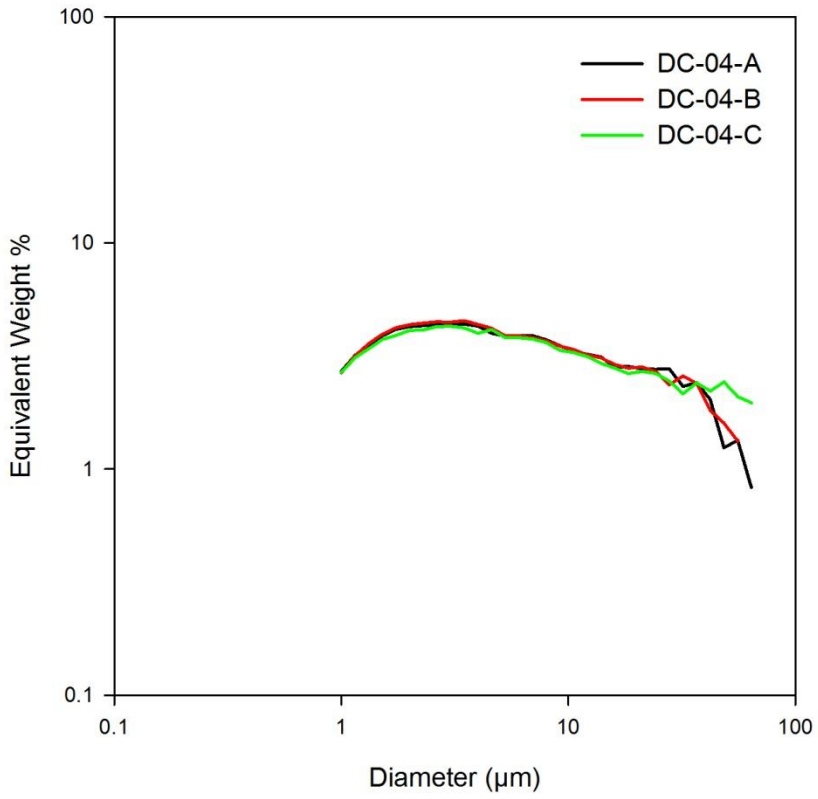

Figure 3: *Disaggregated inorganic grain size analysis was completed on sediment from Douglas Channel (DC), collected from a location four nautical miles from the top of Douglas Channel at Kitimat; hence the sample name DC-04. Samples were run in triplicate. The results of each shown are here, plotted as the log of equivalent weight (%) versus the log of particle diameter. Particle size spectra are also shown in raw form at right, normalized over the size range.*

Diameter (µm)	DC04 A	DC04 B	DC04 C
1	2.708	2.664	2.673
1.149	3.182	3.166	3.101
1.32	3.536	3.586	3.399
1.516	3.884	3.94	3.736
1.741	4.144	4.208	3.899
2	4.26	4.343	4.096
2.297	4.302	4.414	4.12
2.639	4.352	4.476	4.258
3.031	4.371	4.459	4.277
3.482	4.367	4.524	4.202
4	4.284	4.352	3.983
4.595	3.983	4.184	4.127
5.278	3.876	3.882	3.809
6.063	3.876	3.882	3.809
6.964	3.877	3.81	3.751
8	3.728	3.683	3.619
9.19	3.505	3.495	3.344
10.56	3.304	3.374	3.271
12.13	3.213	3.191	3.136
13.93	3.125	3.1	2.929
16	2.82	2.898	2.794
18.38	2.84	2.79	2.643
21.11	2.769	2.823	2.701
24.25	2.757	2.695	2.642
27.86	2.771	2.356	2.45
32	2.321	2.575	2.149
36.76	2.407	2.394	2.4
42.22	2.029	1.814	2.208
48.5	1.243	1.594	2.428
55.72	1.339	1.329	2.089
64	0.827	0	1.96
73.52	0	0	0
84.45	0	0	0
97.01	0	0	0
111.4	0	0	0
128	0	0	0
147	0	0	0
168.9	0	0	0
194	0	0	0
222.9	0	0	0
256	0	0	0
294.1	0	0	0

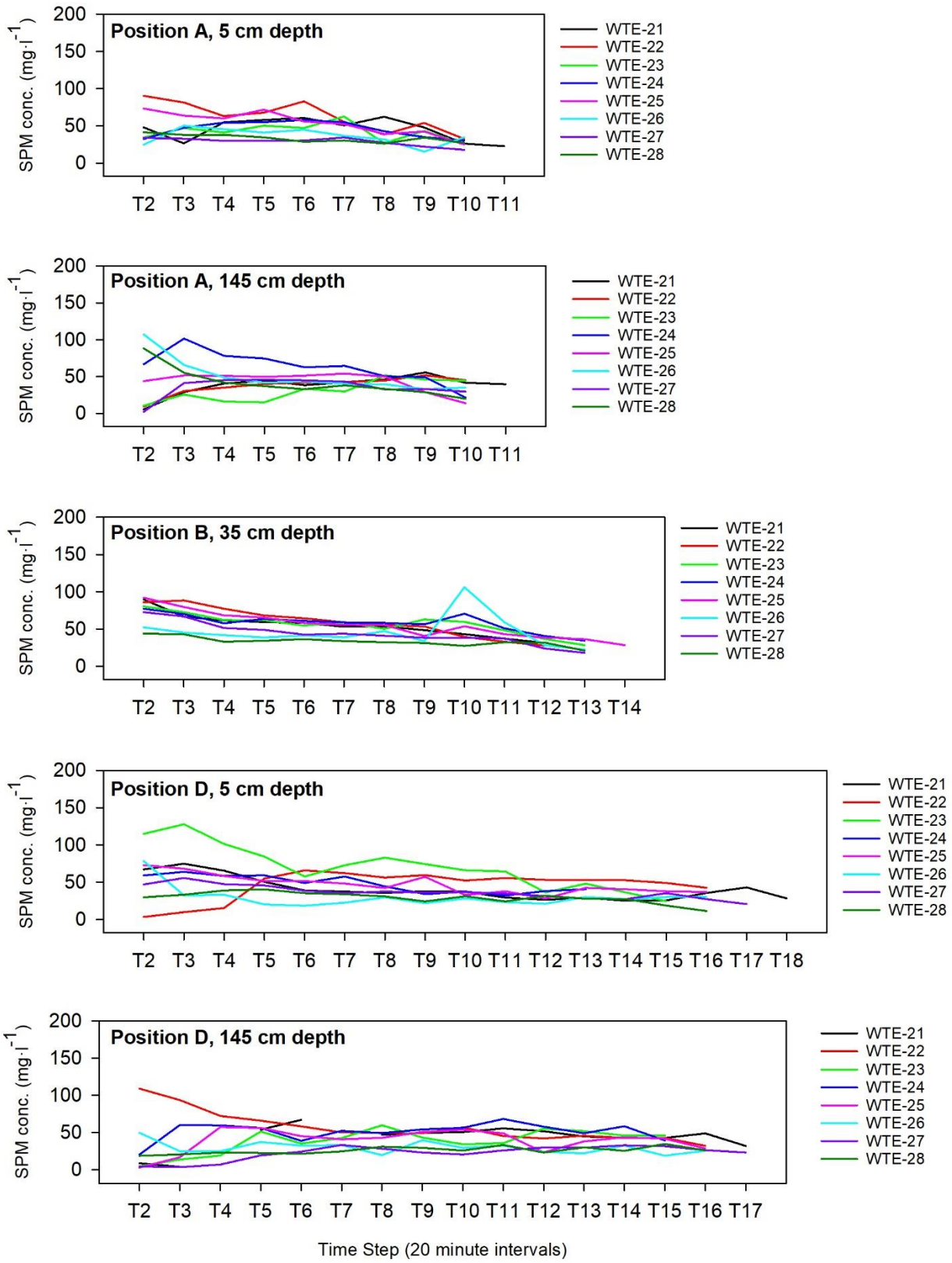

Figure 4: *Changes in SPM concentration (mg·l^{-1}) measured via water samples, at multiple depths at three locations along the wave tank, for the full duration of experiments. Sampling frequency was reduced at Positions A & B during settling, and sampling density at Position D was increased during settling – note variations in X-axis values.*

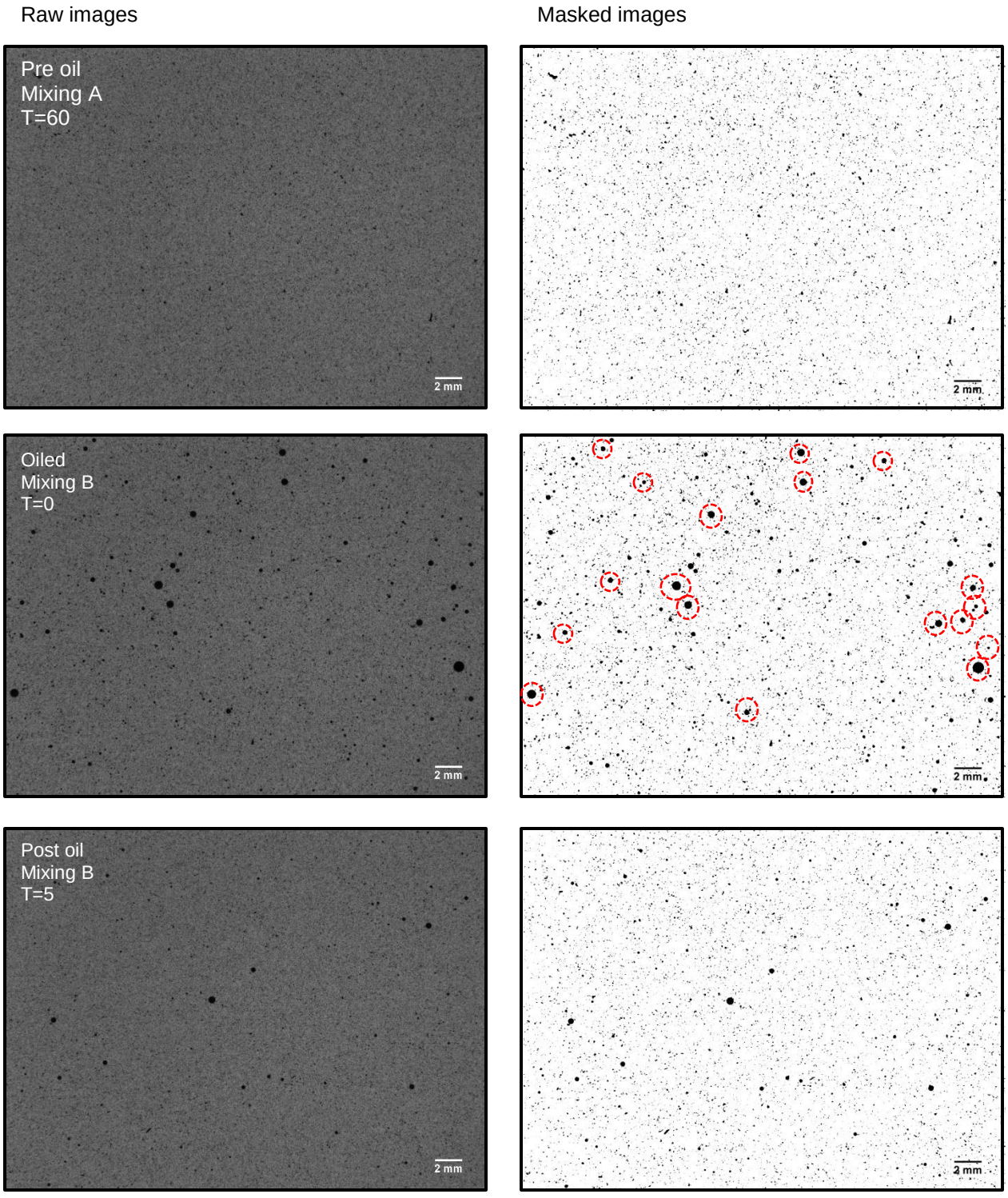

Figure 5: *WTE-21 raw (left) and masked (right) MVFC images, for pre-oil (Mixing A, T=60), oiled (Mixing B, T=0) and post-oil conditions (Mixing B, T=5). Red circles in masked oiled image highlight a number of oil droplets of various sizes that are visually identifiable.*

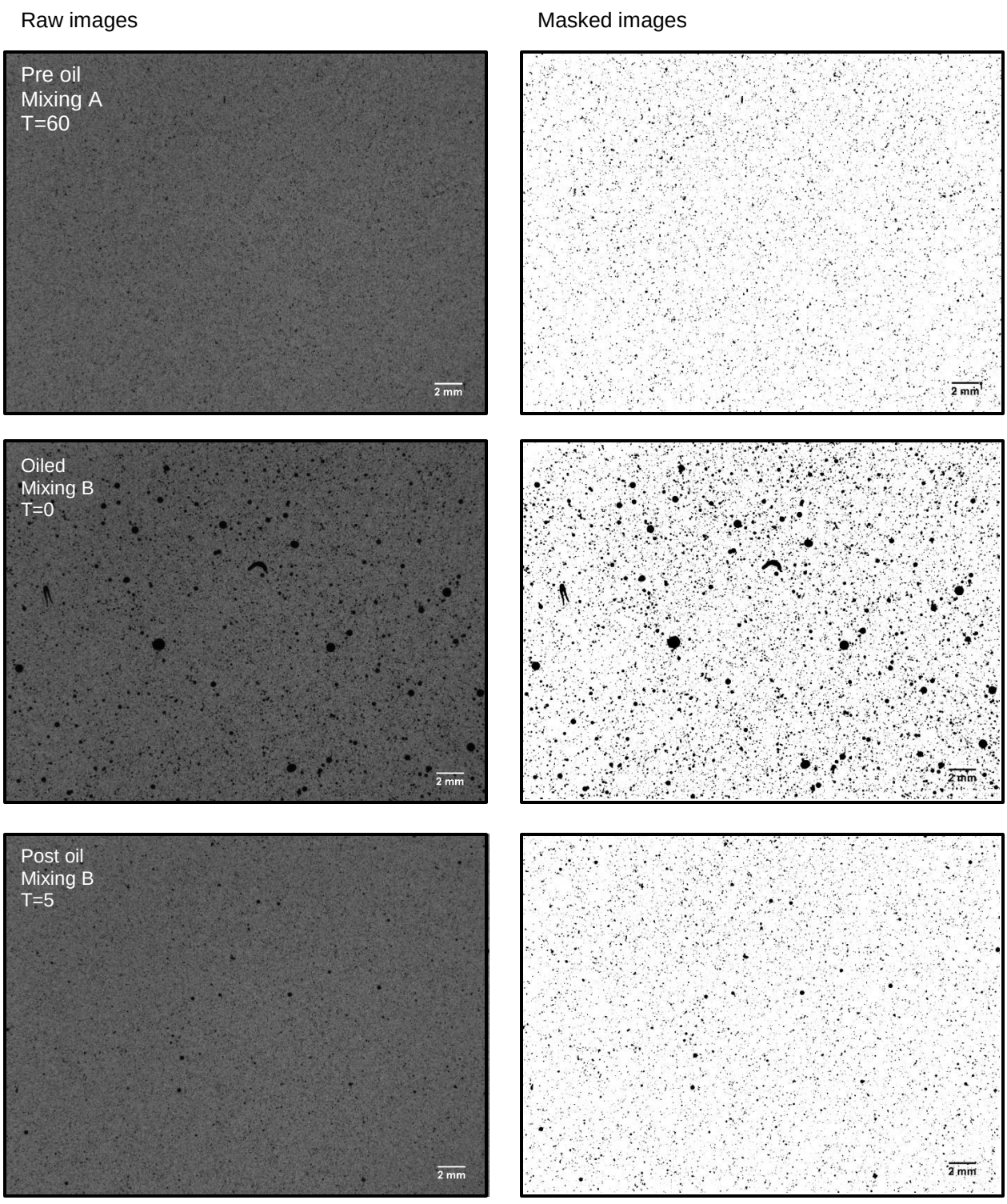

Figure 6: *WTE-22 raw (left) and masked (right) MVFC images, for pre-oil (Mixing A, T=60), oiled (Mixing B, T=0) and post-oil conditions (Mixing B, T=5).*

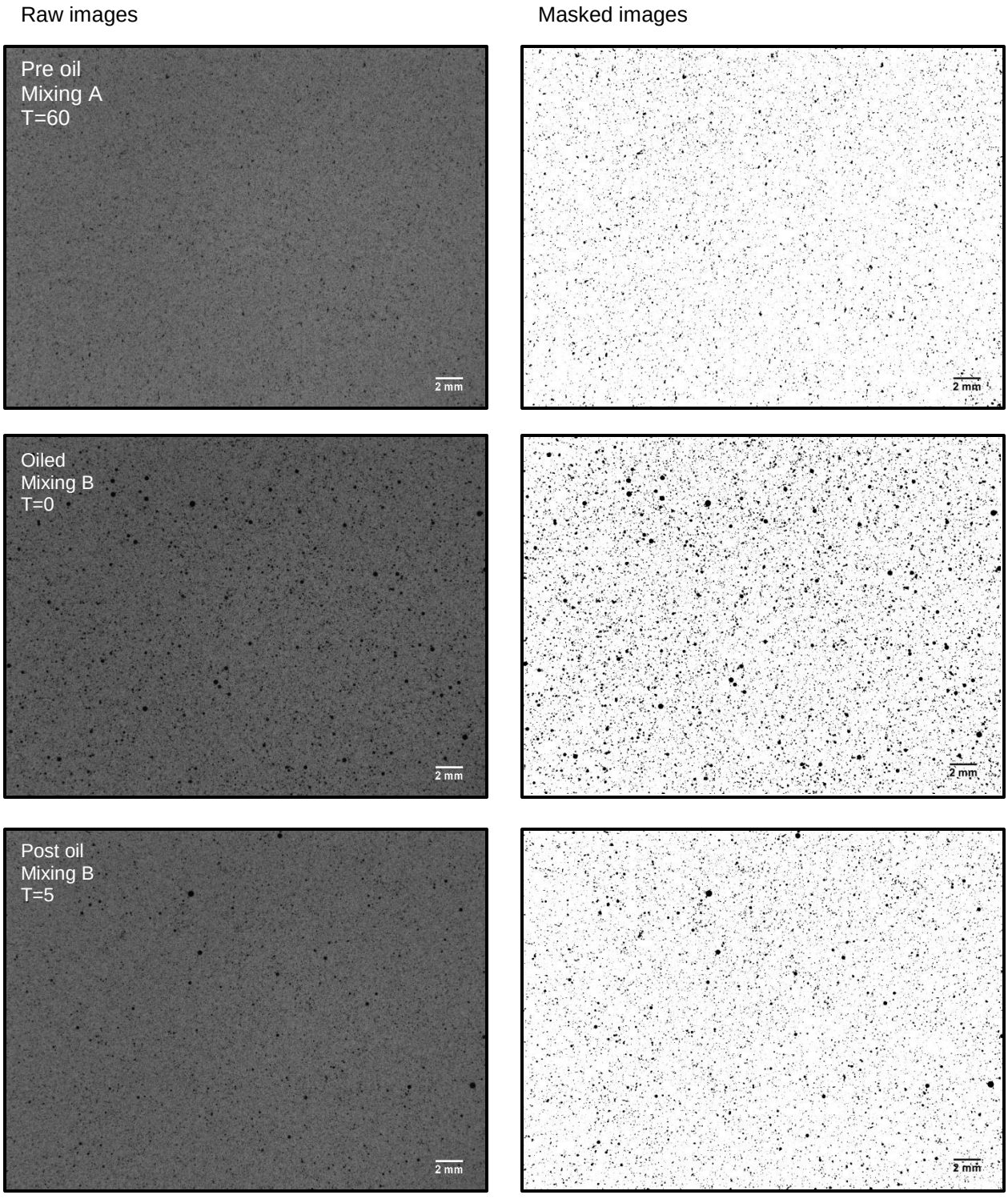

Figure 7: *WTE-23 raw (left) and masked (right) MVFC images, for pre-oil (Mixing A, T=60), oiled (Mixing B, T=0) and post-oil conditions (Mixing B, T=5).*

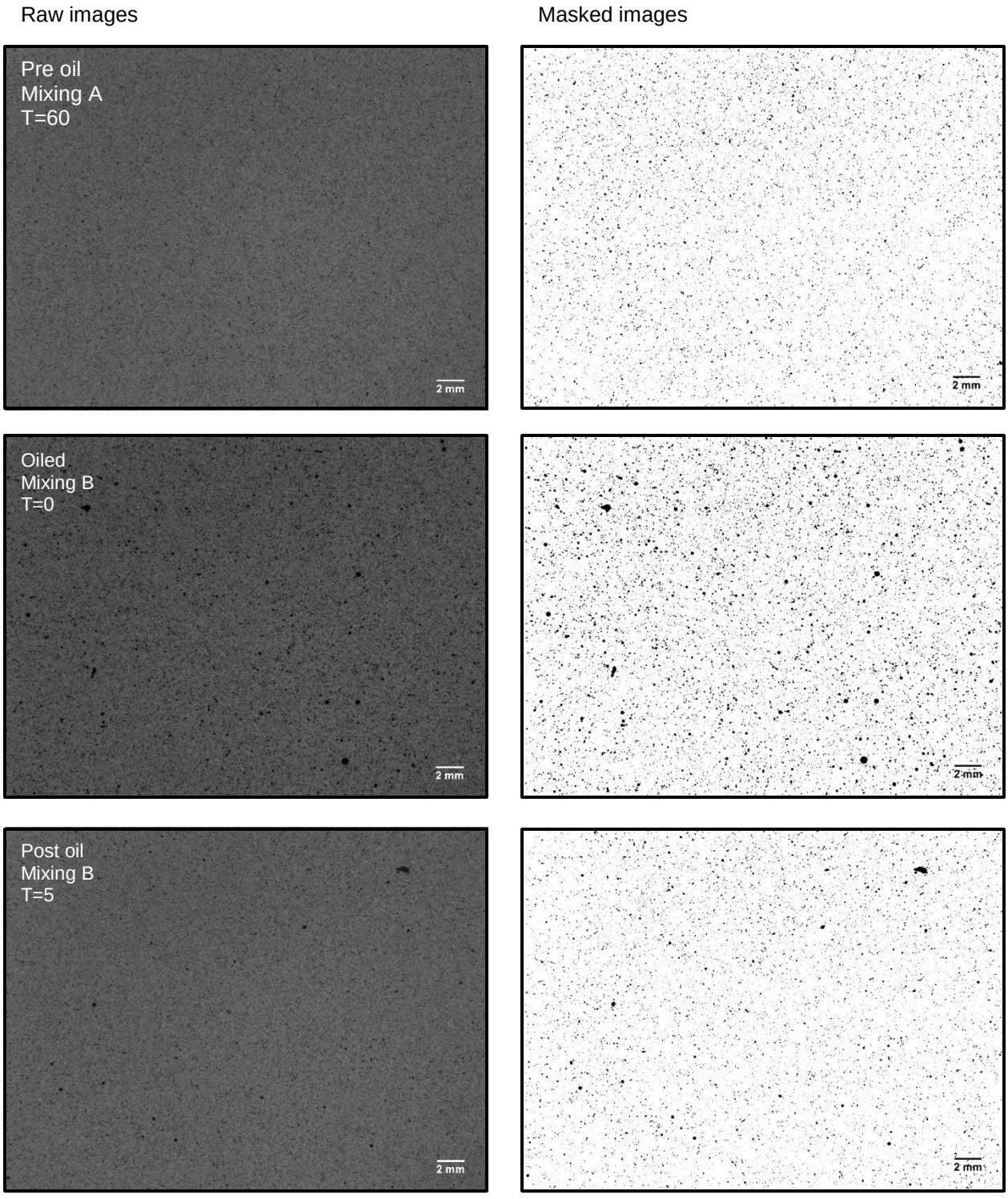

Figure 8: *WTE-24 raw (left) and masked (right) MVFC images, for pre-oil (Mixing A, T=60), oiled (Mixing B, T=0) and post-oil conditions (Mixing B, T=5).*

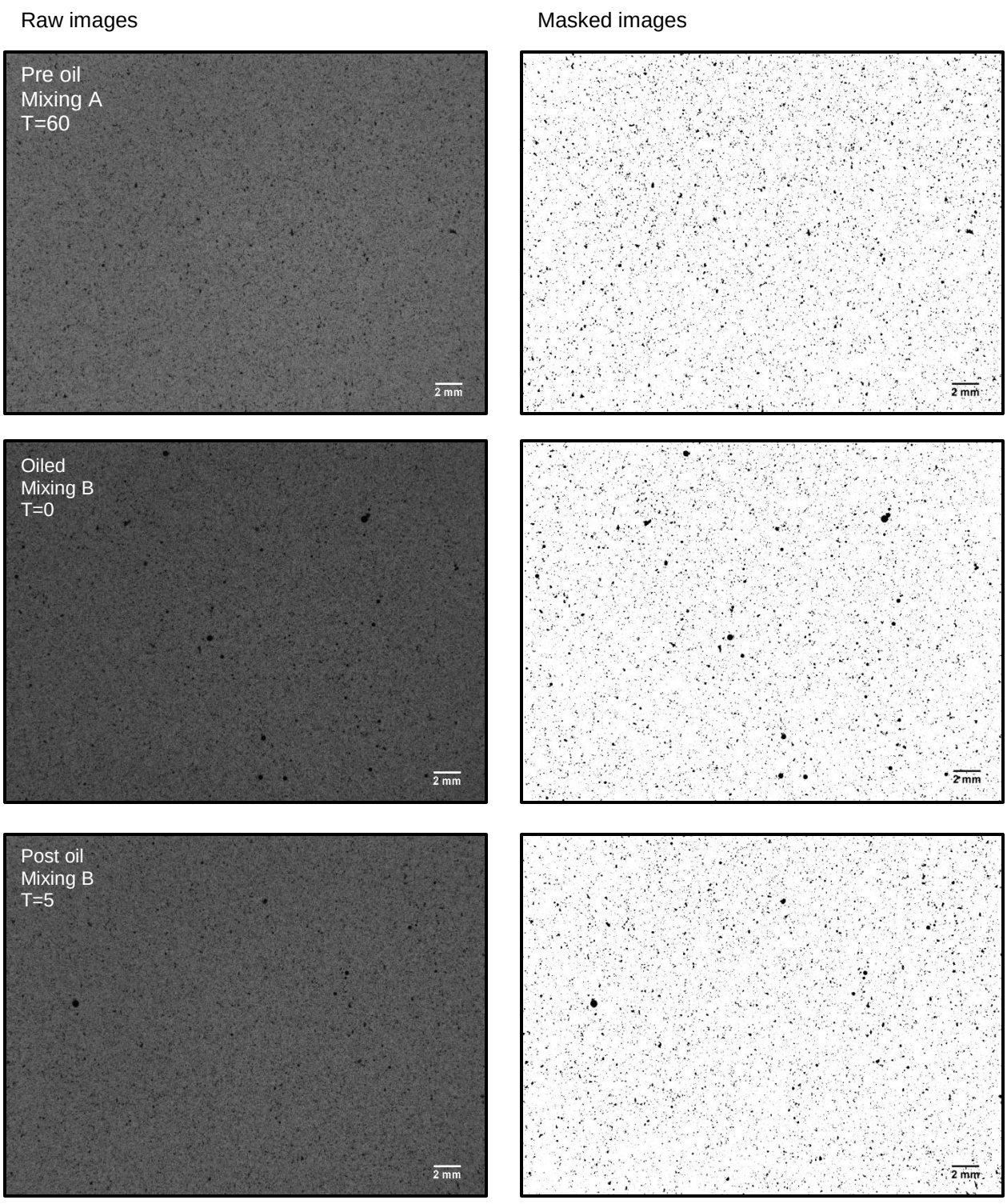

Figure 9: *WTE-25 raw (left) and masked (right) MVFC images, for pre-oil (Mixing A, T=60), oiled (Mixing B, T=0) and post-oil conditions (Mixing B, T=5).*

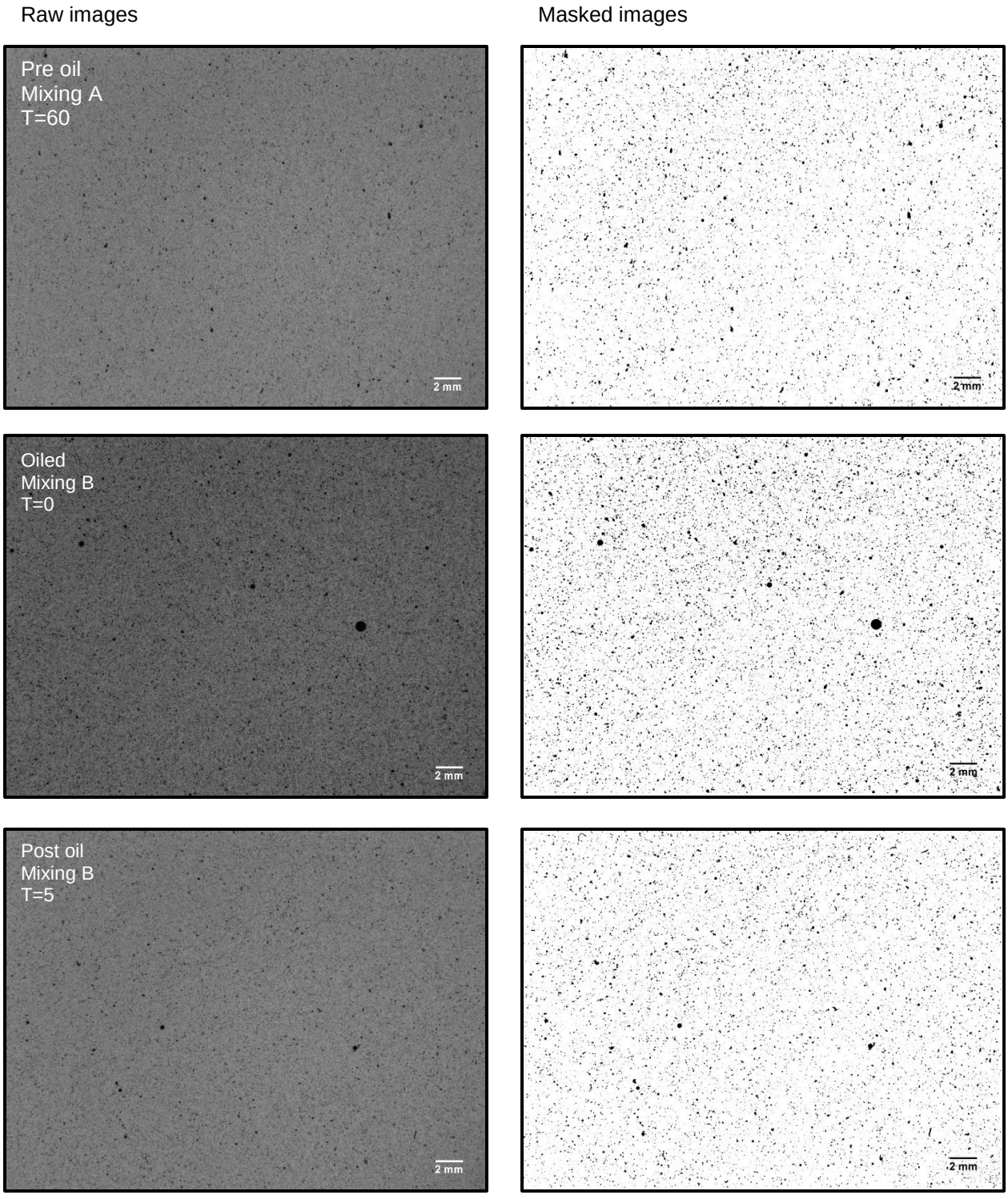

Figure 10: *WTE-26 raw (left) and masked (right) MVFC images, for pre-oil (Mixing A, T=60), oiled (Mixing B, T=0) and post-oil conditions (Mixing B, T=5).*

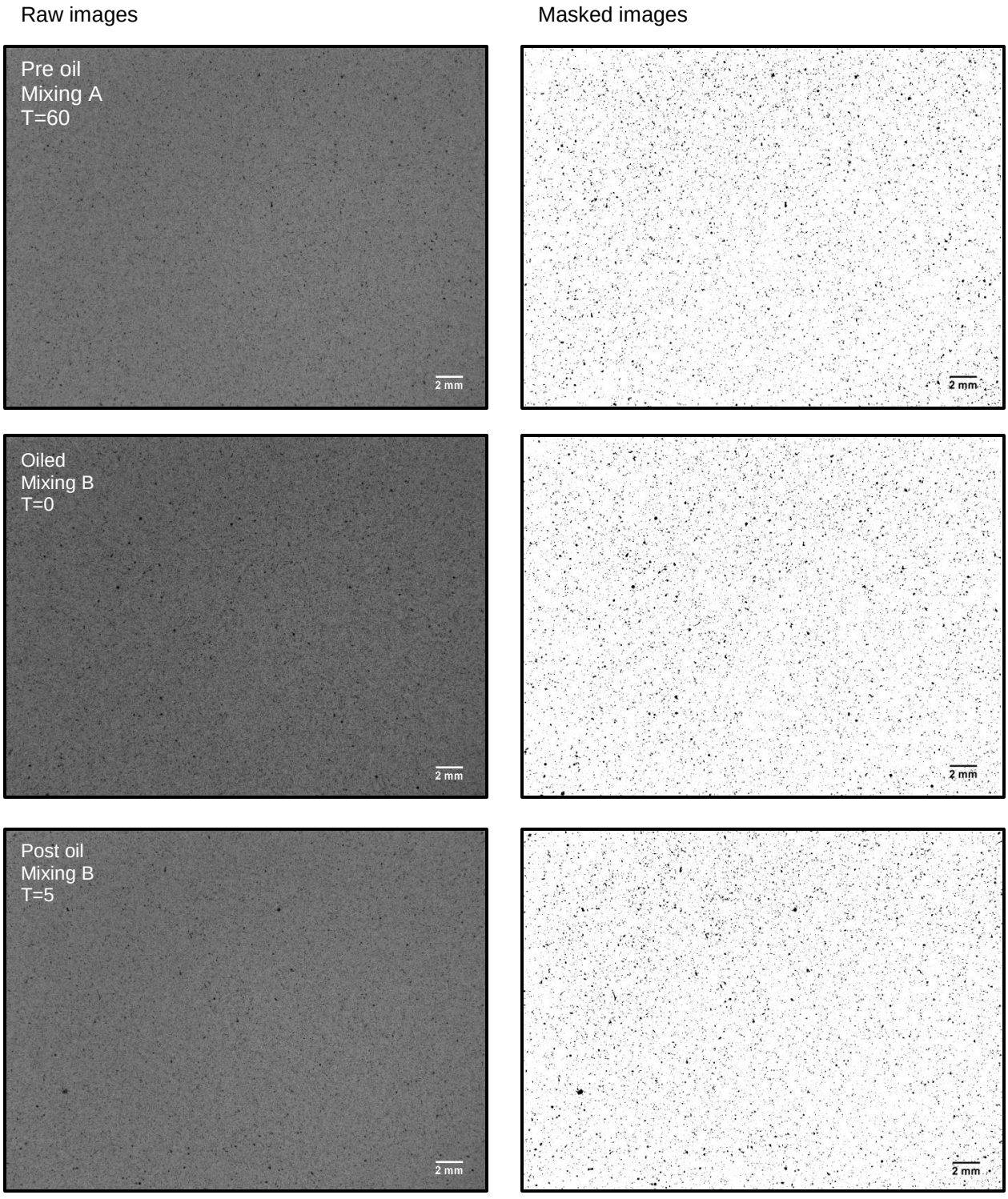

Figure 11: *WTE-27 raw (left) and masked (right) MVFC images, for pre-oil (Mixing A, T=60), oiled (Mixing B, T=0) and post-oil conditions (Mixing B, T=5).*

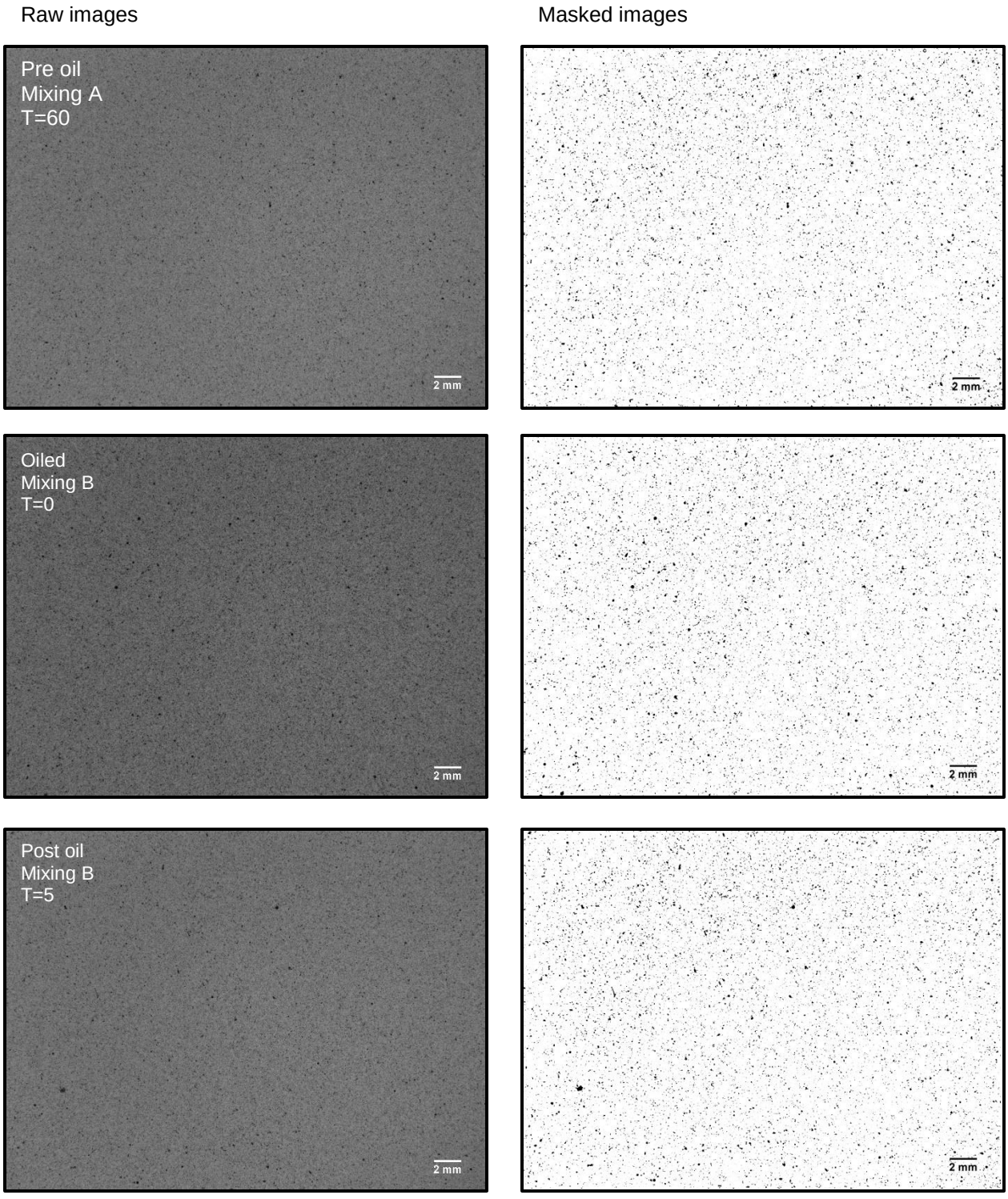

Figure 12: *WTE-28 raw (left) and masked (right) MVFC images, for pre-oil (Mixing A, T=60), oiled (Mixing B, T=0) and post-oil conditions (Mixing B, T=5).*

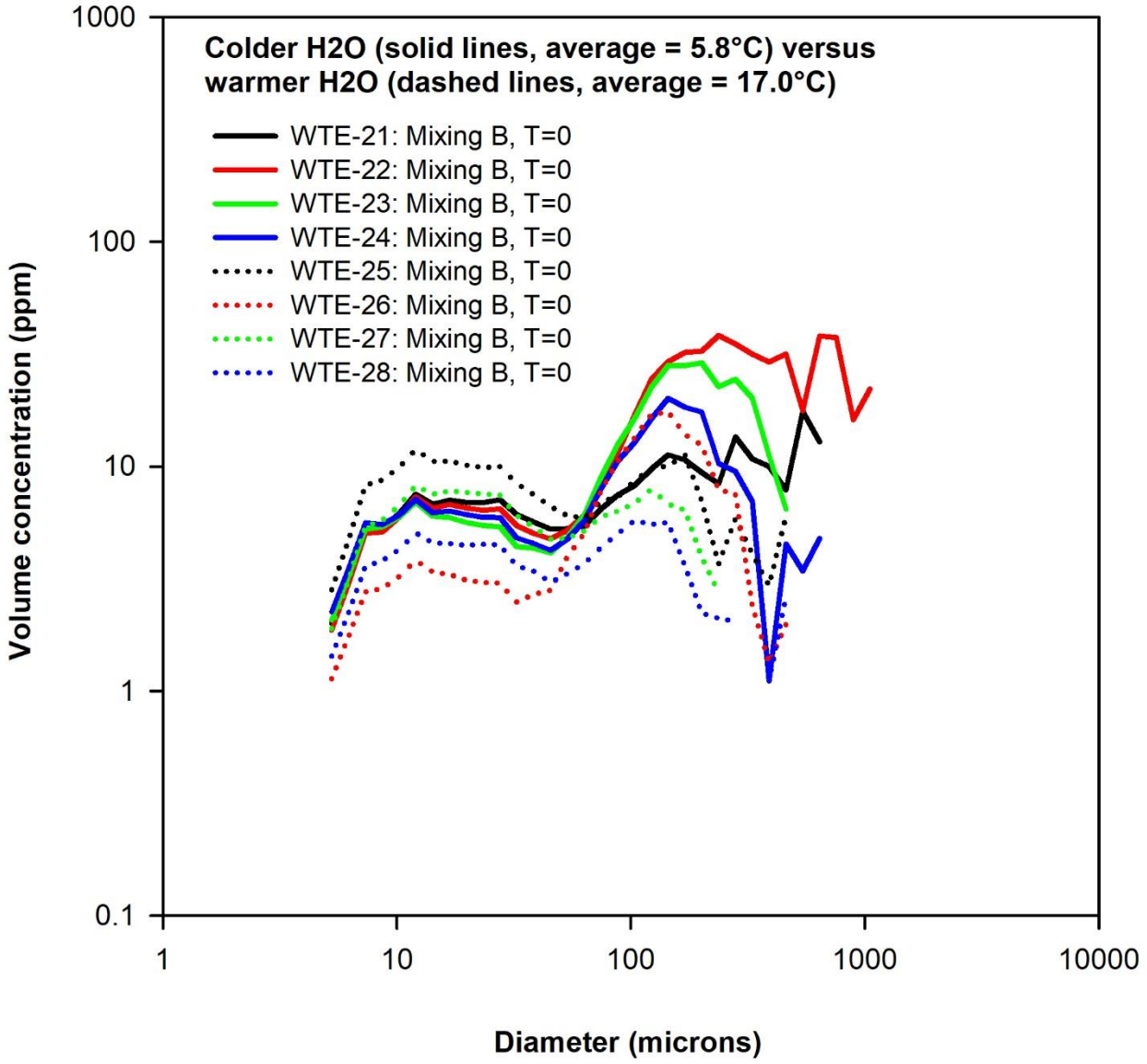

Figure 13: *An overlay comparison of merged size spectra from the MVFC & LISST, immediately following the addition of dispersed oil to the tank (Mixing B, T=0). Data are plotted as the log of volume concentration (ppm) versus the log of particle diameter (µm).*

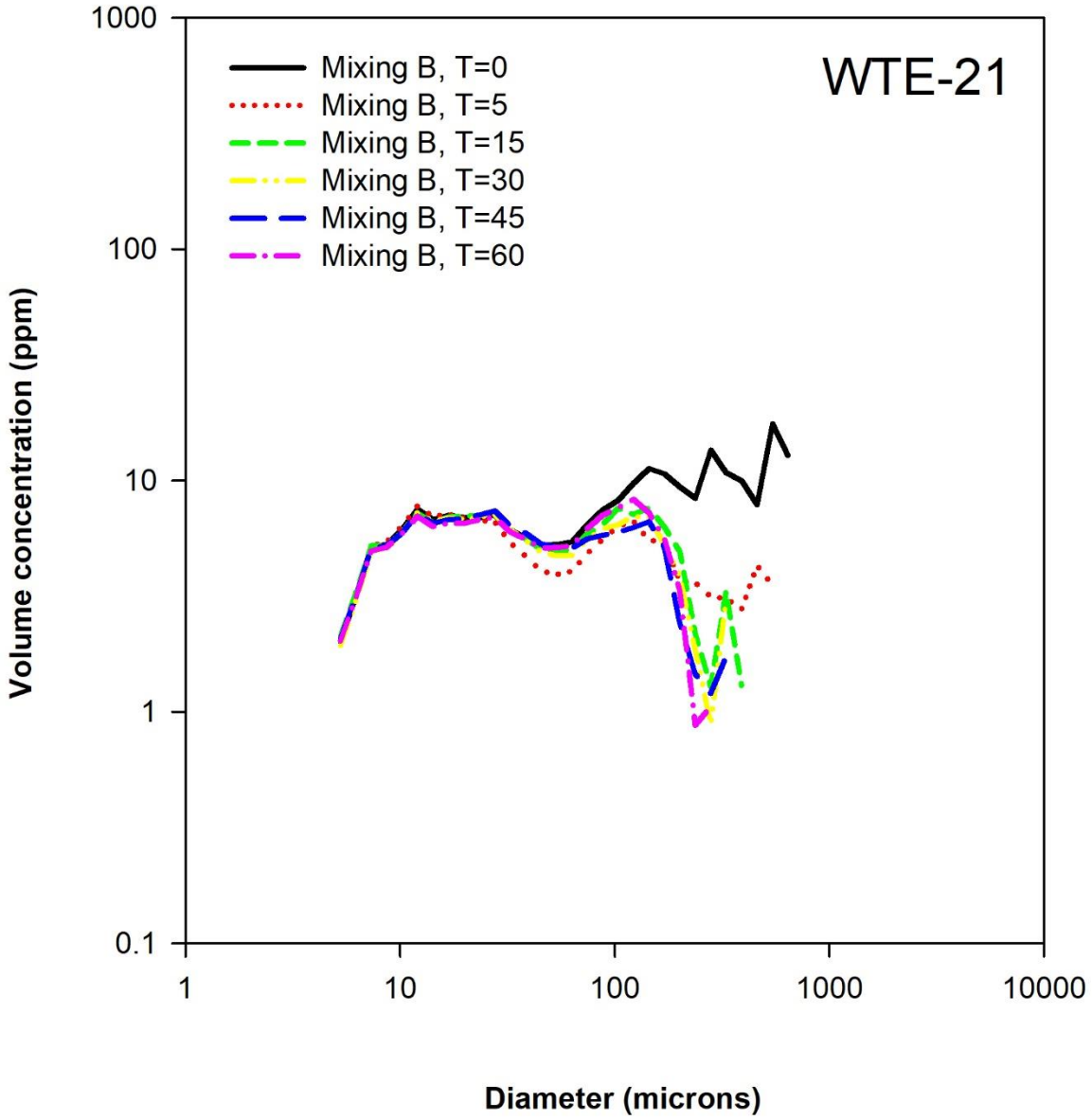

Figure 14: *Merged size spectra from the MVFC & LISST, characterizing the mixing B phase of WTE-21, at 5 and 15 minute increments. Data are plotted as the log of volume concentration (ppm) versus the log of particle diameter (µm).*

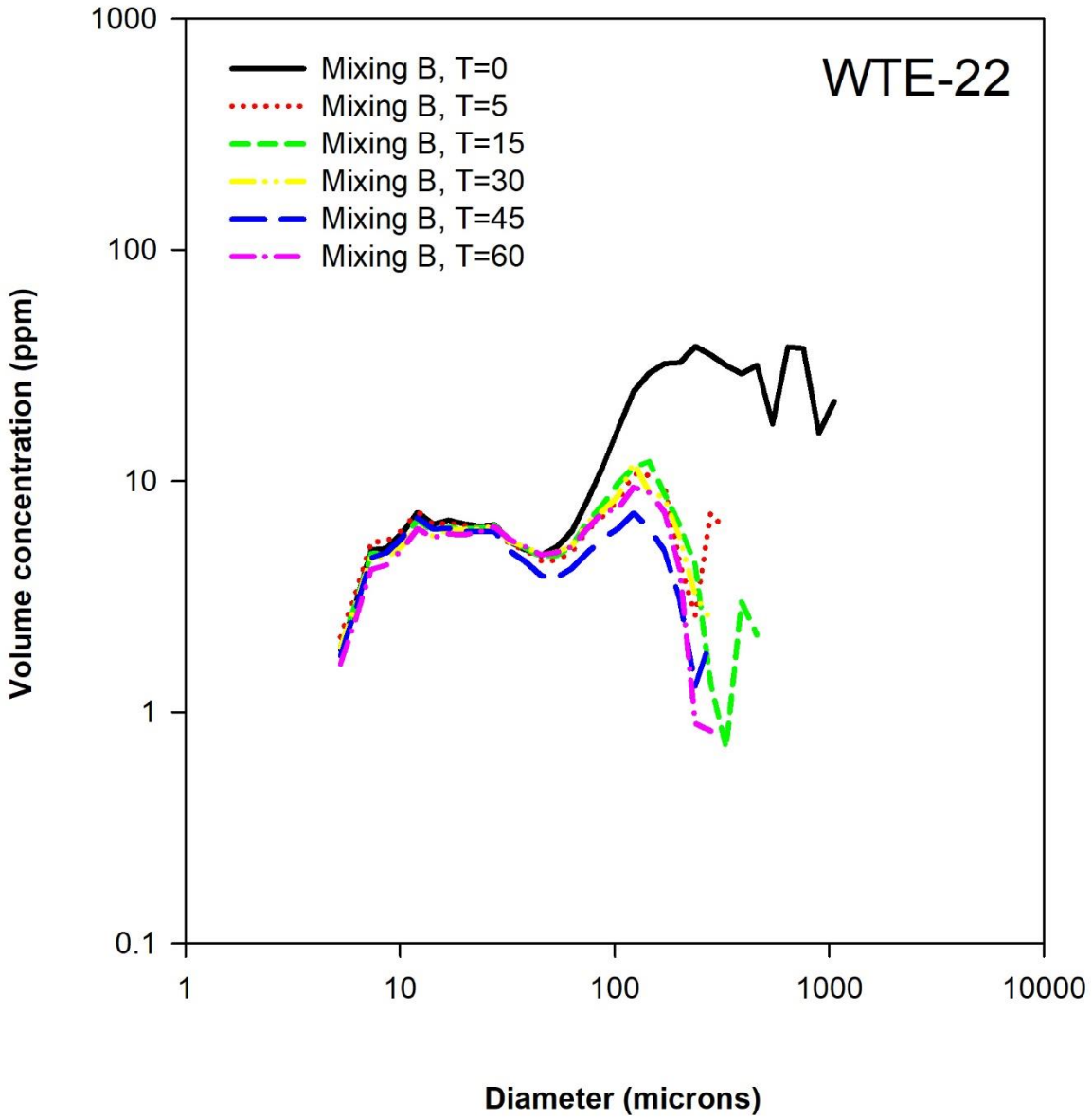

Figure 15: *Merged size spectra from the MVFC & LISST, characterizing the mixing B phase of WTE-22, at 5 and 15 minute increments. Data are plotted as the log of volume concentration (ppm) versus the log of particle diameter (µm).*

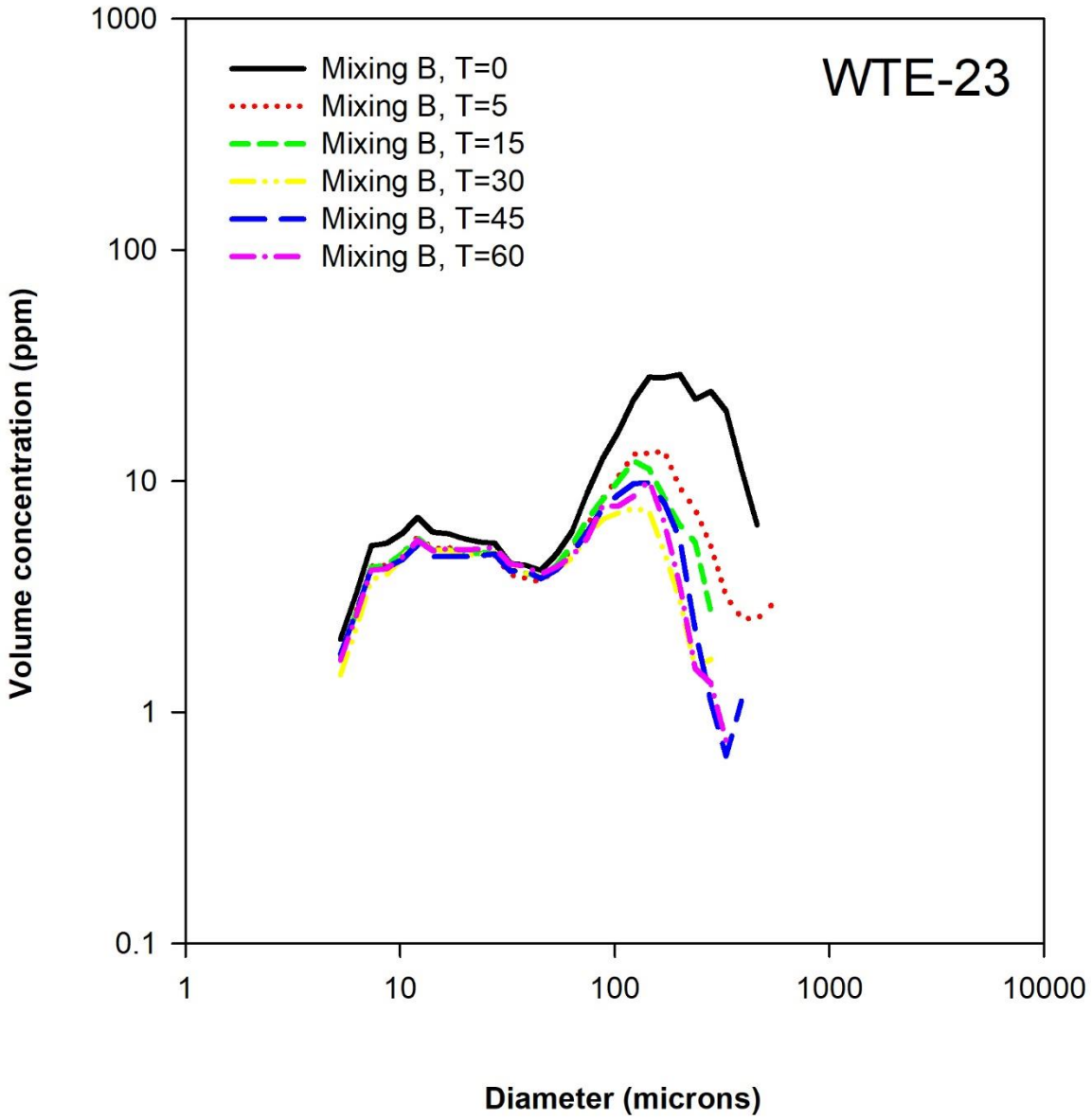

Figure 16: *Merged size spectra from the MVFC & LISST, characterizing the mixing B phase of WTE-23, at 5 and 15 minute increments. Data are plotted as the log of volume concentration (ppm) versus the log of particle diameter (µm).*

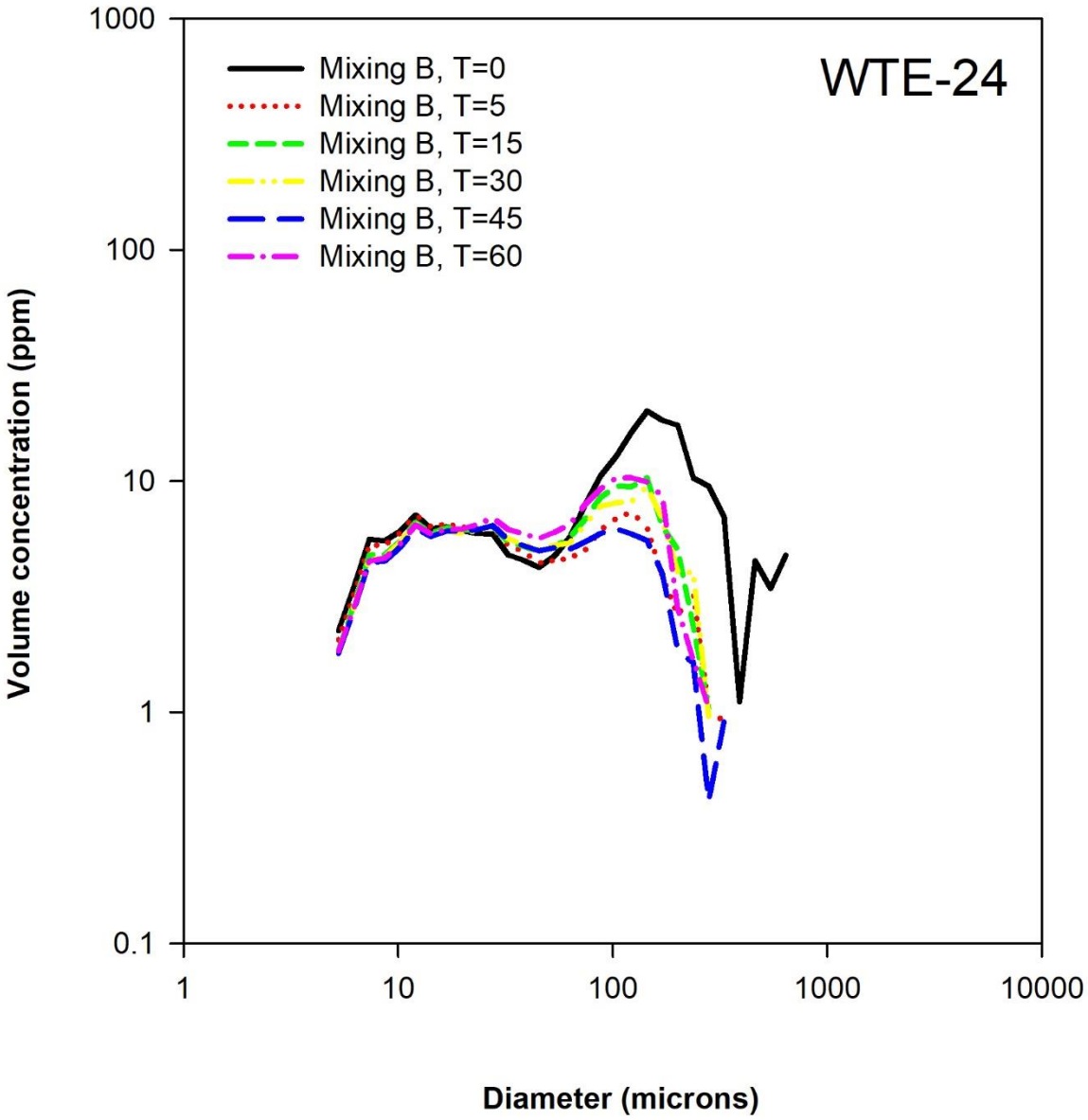

Figure 17: *Merged size spectra from the MVFC & LISST, characterizing the mixing B phase of WTE-24, at 5 and 15 minute increments. Data are plotted as the log of volume concentration (ppm) versus the log of particle diameter (µm).*

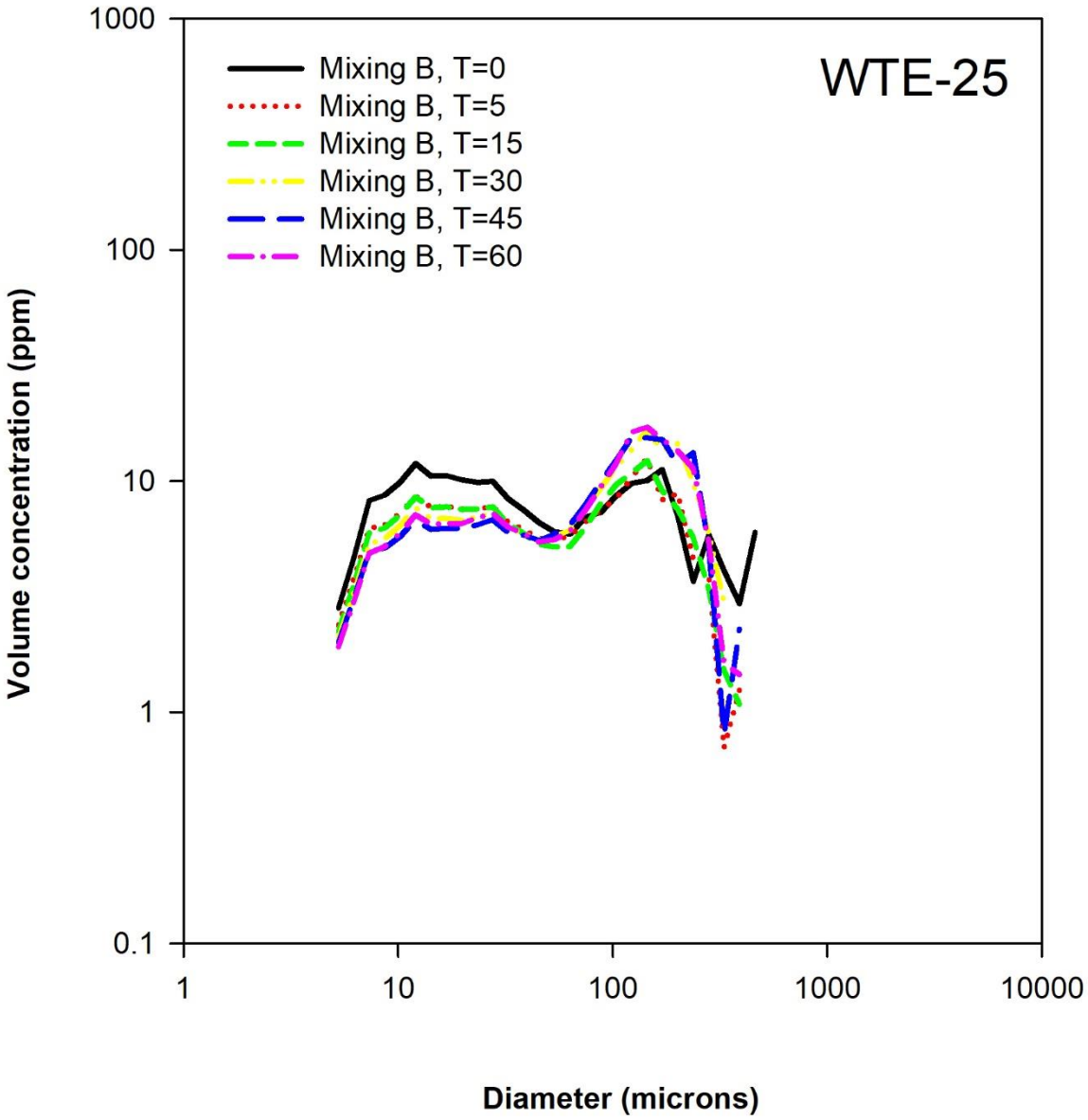

Figure 18: *Merged size spectra from the MVFC & LISST, characterizing the mixing B phase of WTE-25, at 5 and 15 minute increments. Data are plotted as the log of volume concentration (ppm) versus the log of particle diameter (µm).*

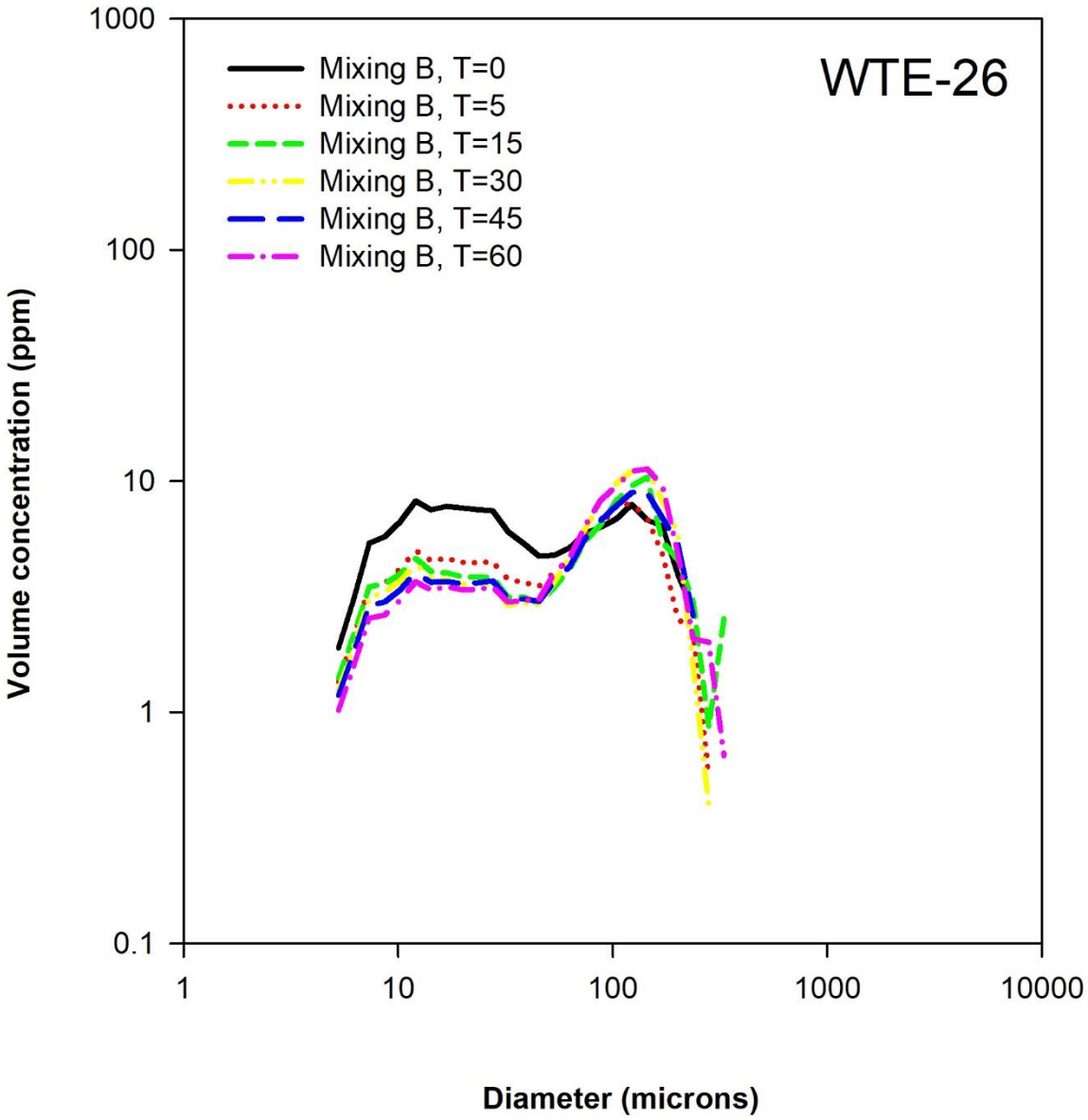

Figure 19: *Merged size spectra from the MVFC & LISST, characterizing the mixing B phase of WTE-26, at 5 and 15 minute increments. Data are plotted as the log of volume concentration (ppm) versus the log of particle diameter (µm).*

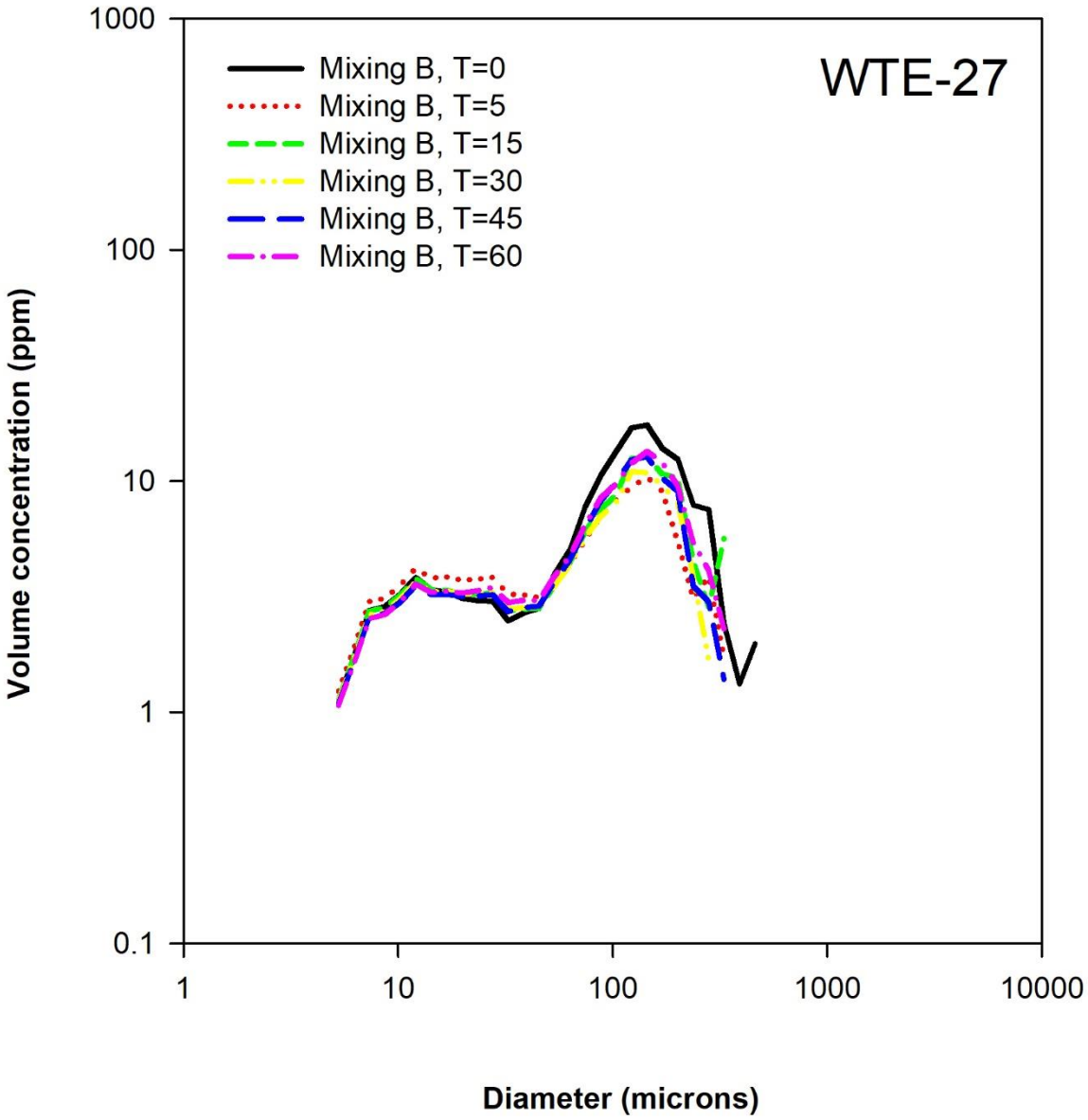

Figure 20: *Merged size spectra from the MVFC & LISST, characterizing the mixing B phase of WTE-27, at 5 and 15 minute increments. Data are plotted as the log of volume concentration (ppm) versus the log of particle diameter (µm).*

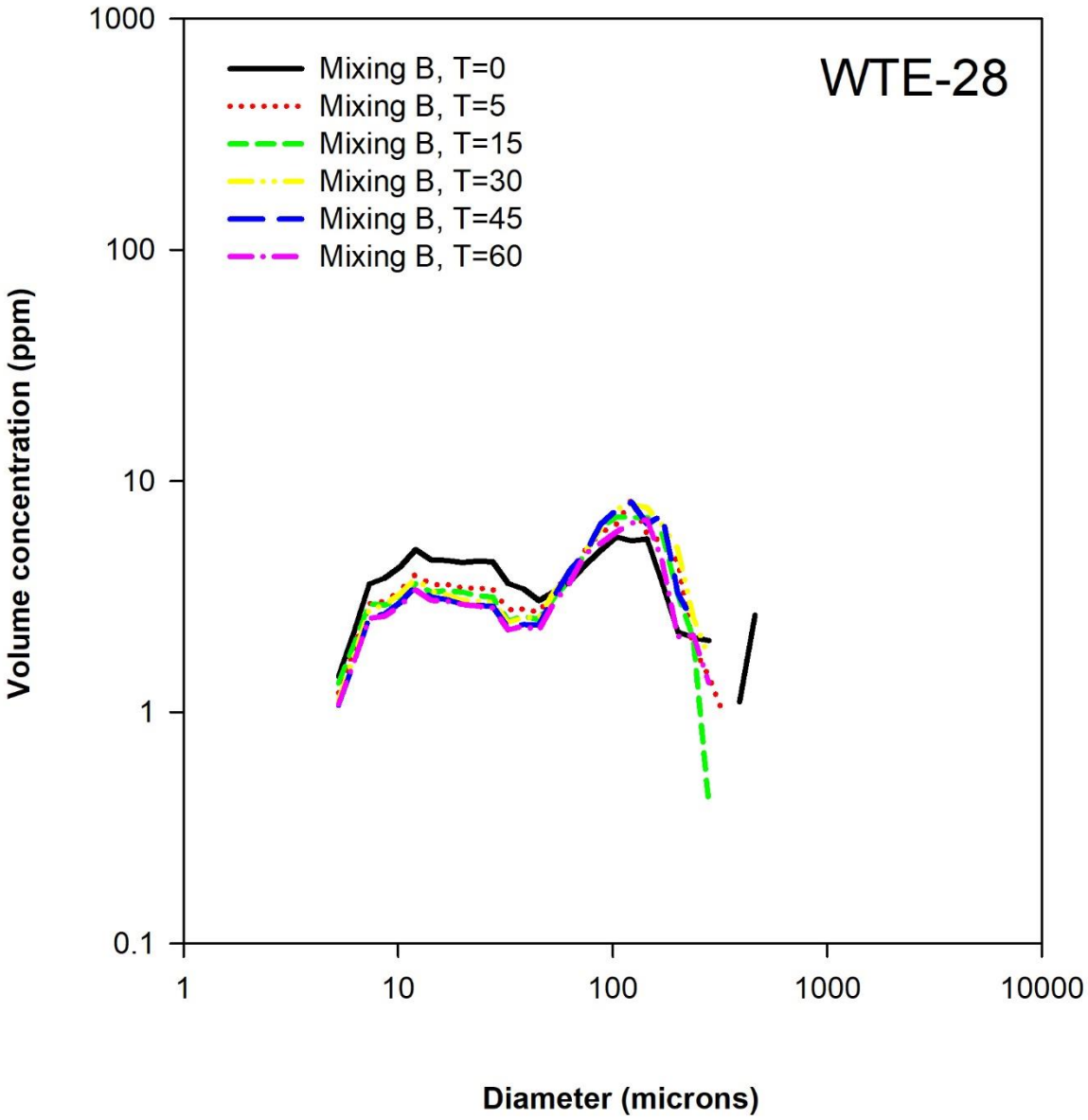

Figure 21: *Merged size spectra from the MVFC & LISST, characterizing the mixing B phase of WTE-28, at 5 and 15 minute increments. Data are plotted as the log of volume concentration (ppm) versus the log of particle diameter (µm).*

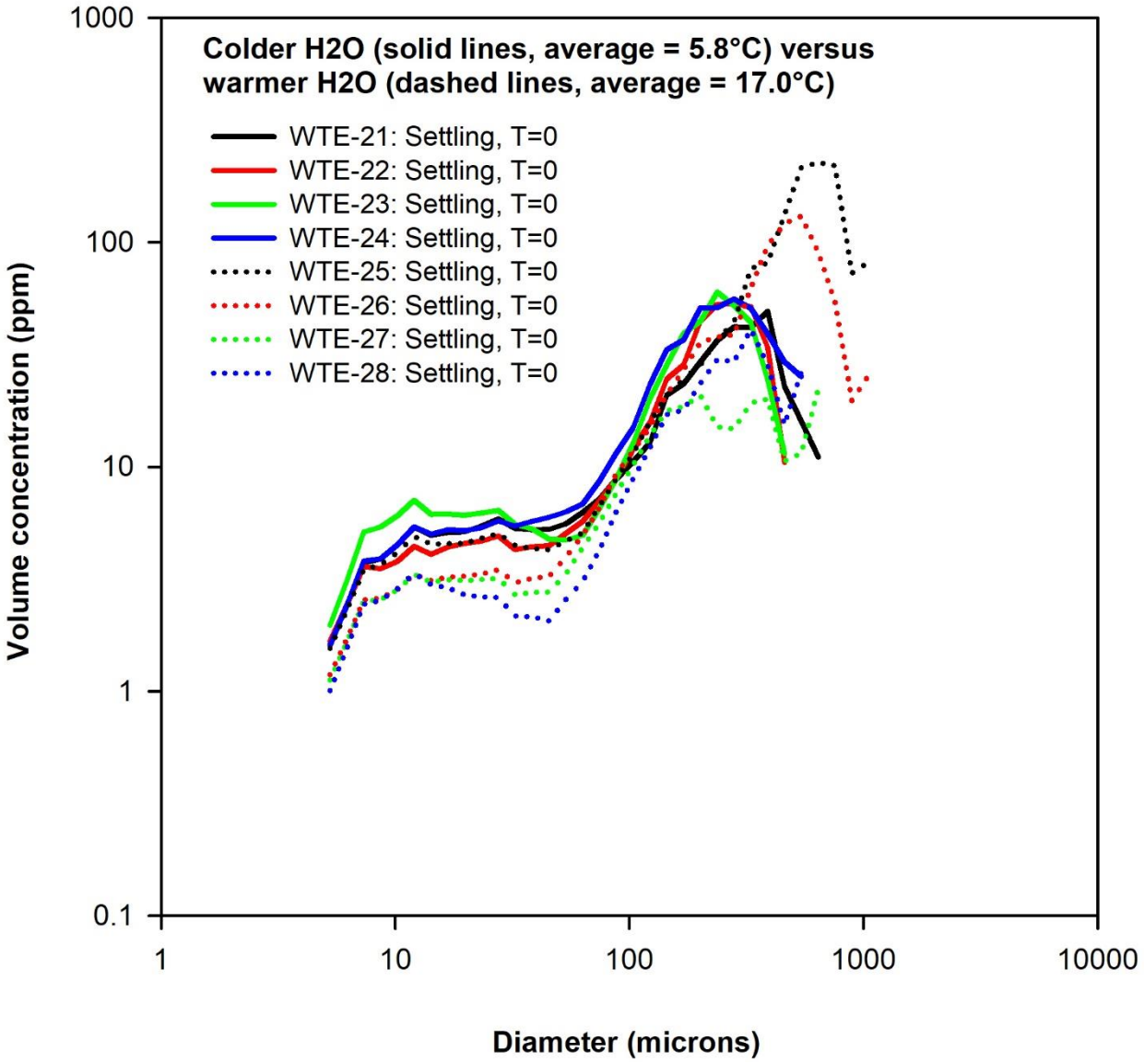

Figure 22: *An overlay comparison of merged size spectra from the MVFC & LISST, settling phase, T=0. Data are plotted as the log of volume concentration (ppm) versus the log of particle diameter (µm).*

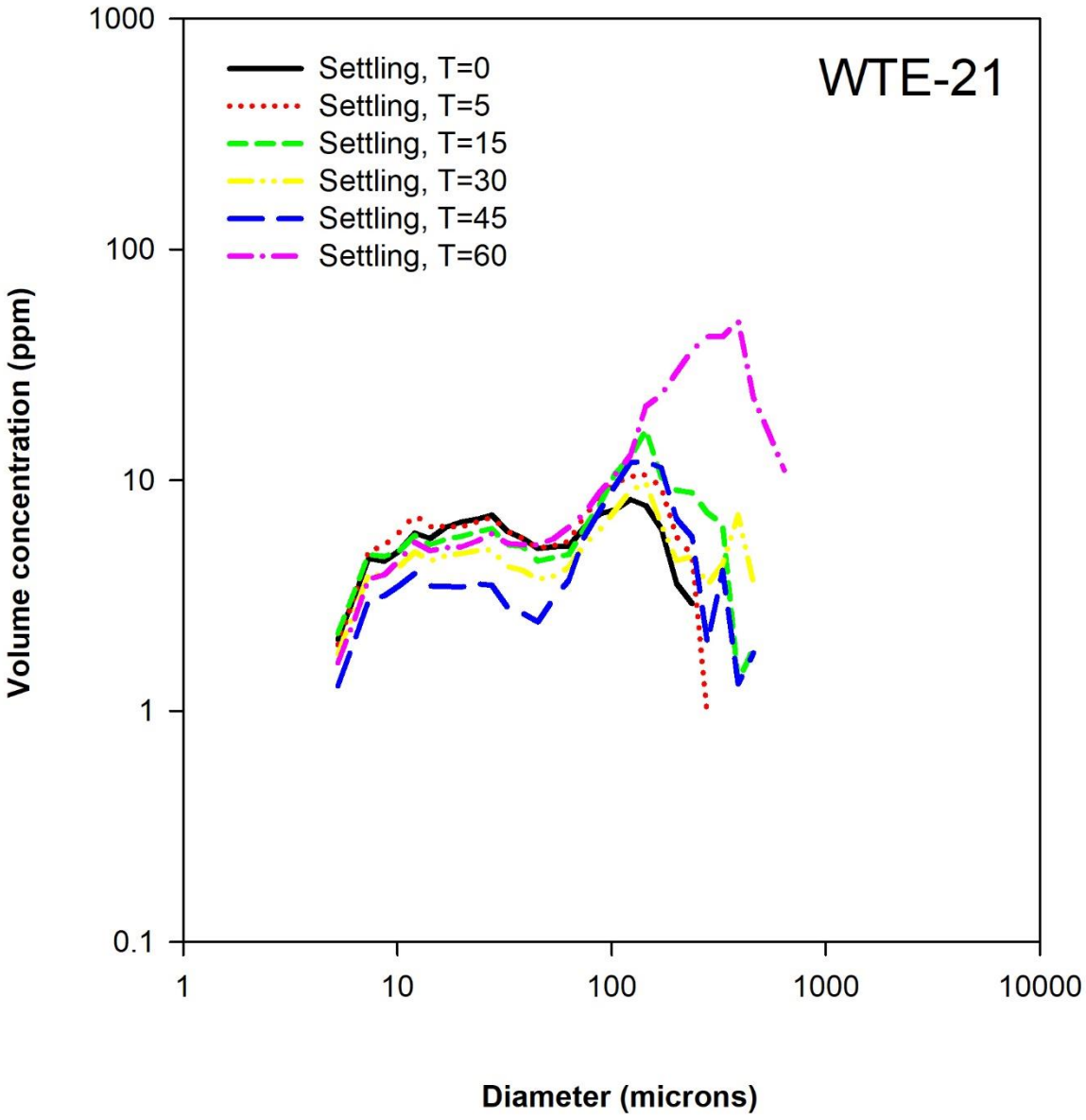

Figure 23: *Merged size spectra from the MVFC & LISST, characterizing the settling phase of WTE-21, at 5 and 15 minute increments. Data are plotted as the log of volume concentration (ppm) versus the log of particle diameter (µm).*

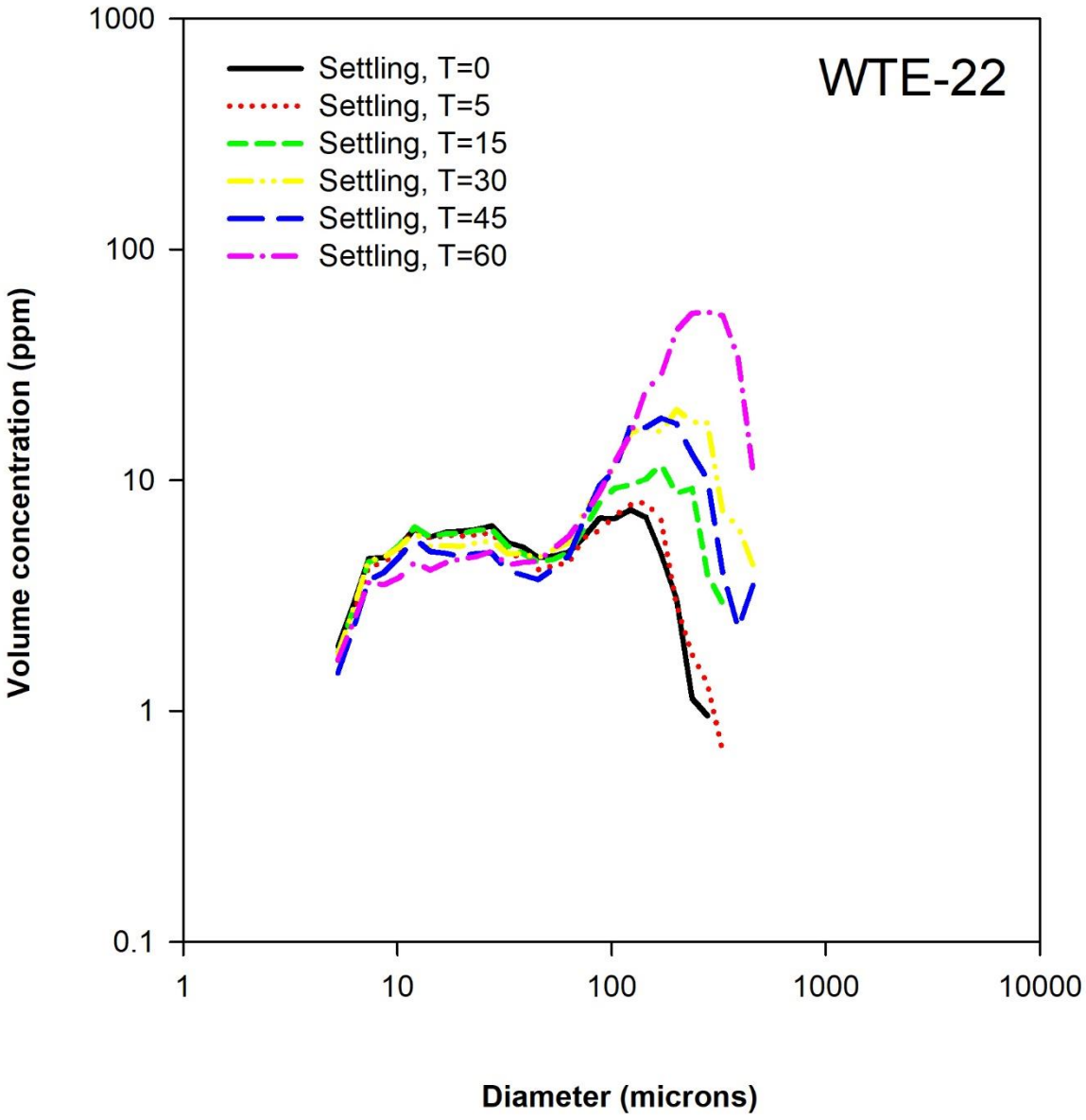

Figure 24: *Merged size spectra from the MVFC & LISST, characterizing the settling phase of WTE-22, at 5 and 15 minute increments. Data are plotted as the log of volume concentration (ppm) versus the log of particle diameter (µm).*

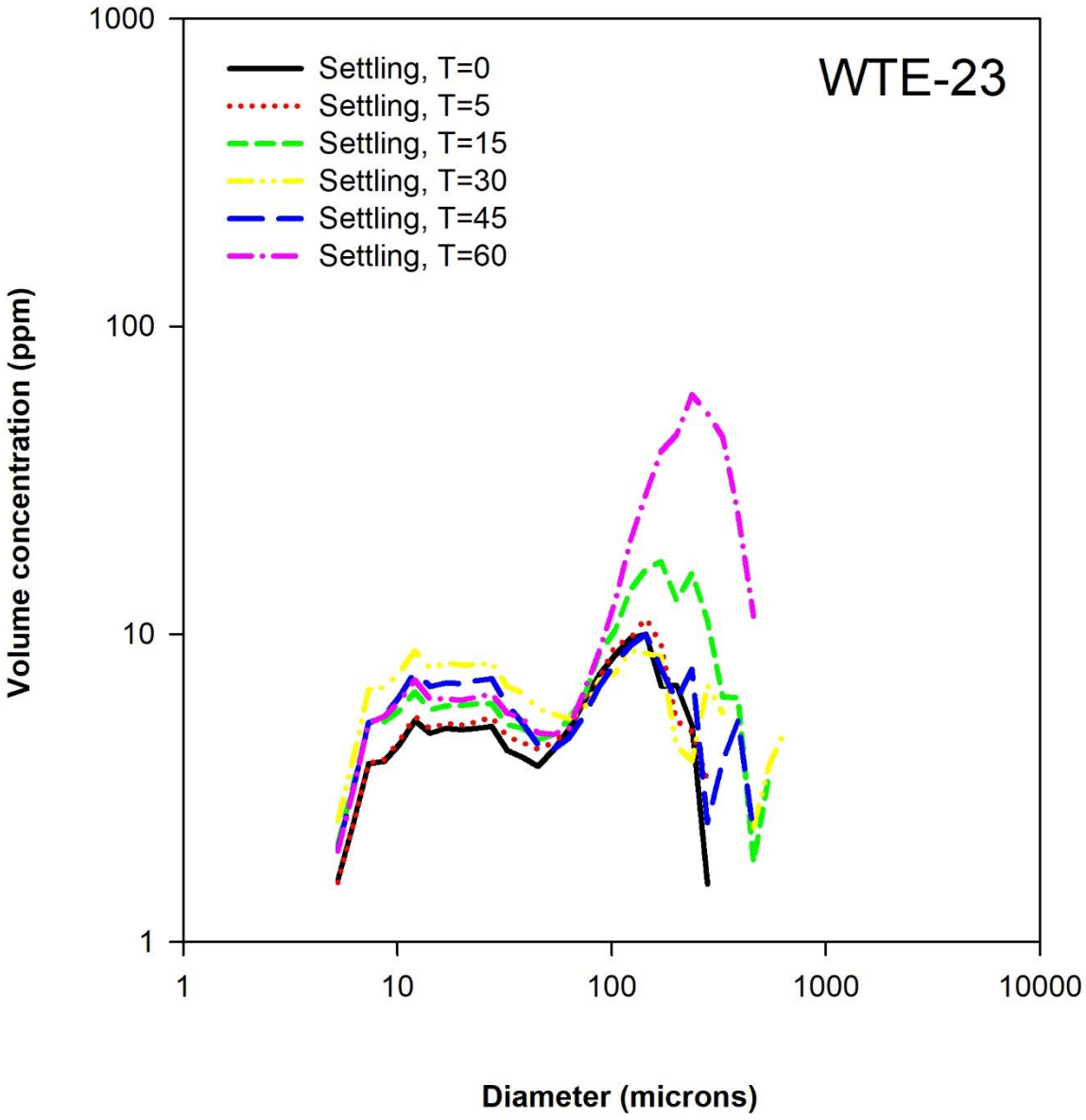

Figure 25: *Merged size spectra from the MVFC & LISST, characterizing the settling phase of WTE-23, at 5 and 15 minute increments. Data are plotted as the log of volume concentration (ppm) versus the log of particle diameter (µm).*

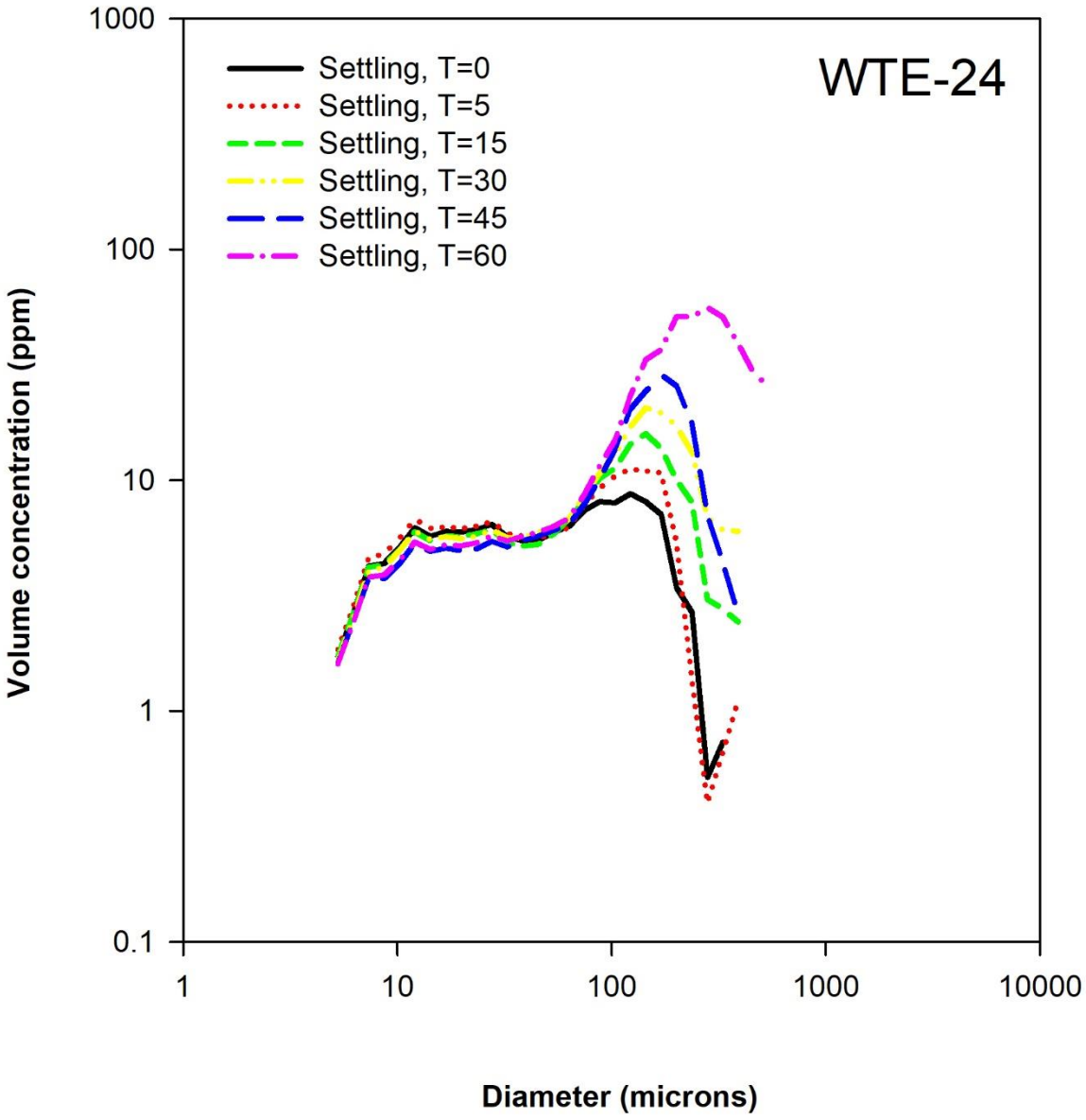

Figure 26: *Merged size spectra from the MVFC & LISST, characterizing the settling phase of WTE-24, at 5 and 15 minute increments. Data are plotted as the log of volume concentration (ppm) versus the log of particle diameter (µm).*

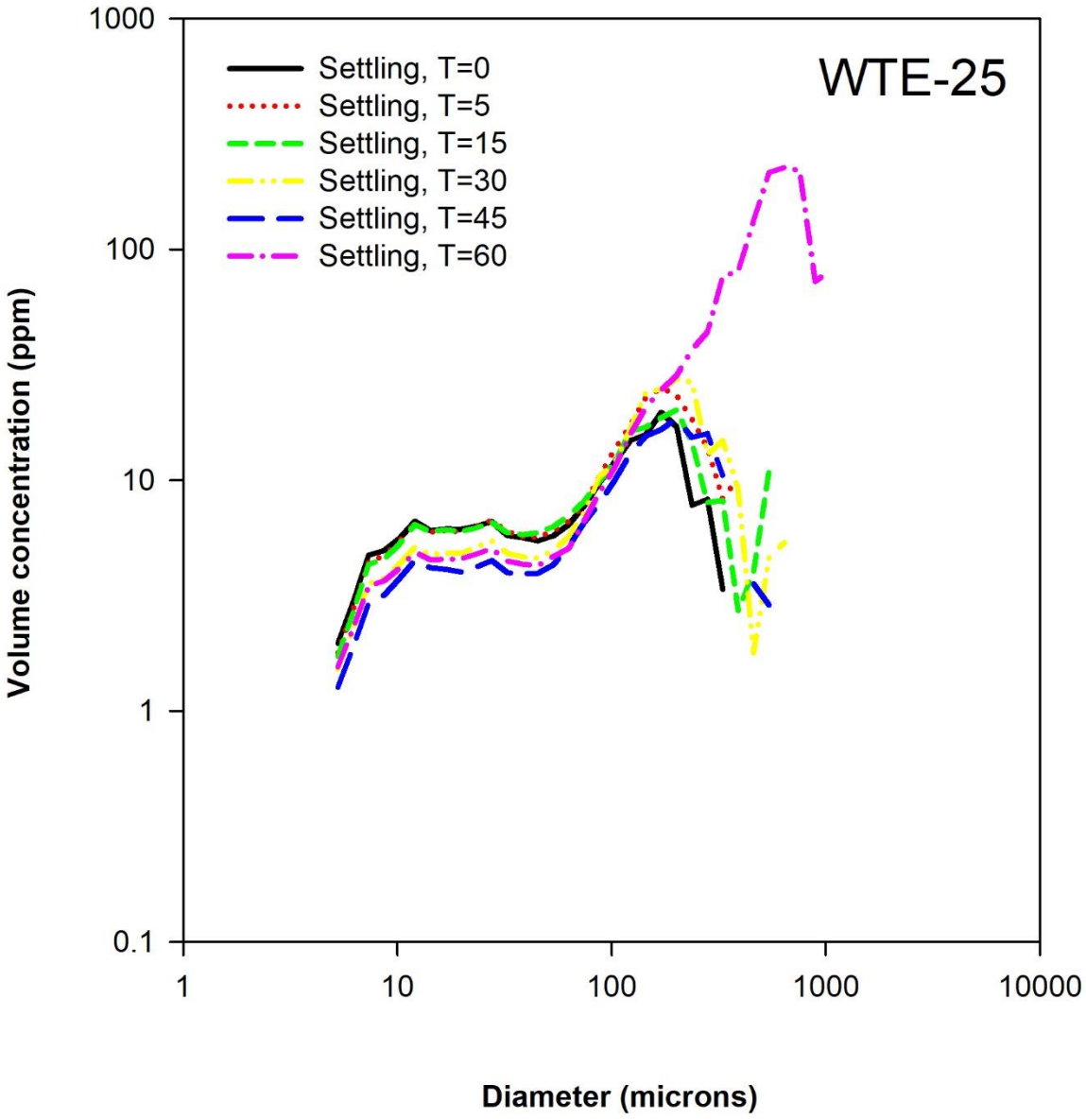

Figure 27: *Merged size spectra from the MVFC & LISST, characterizing the settling phase of WTE-25, at 5 and 15 minute increments. Data are plotted as the log of volume concentration (ppm) versus the log of particle diameter (µm).*

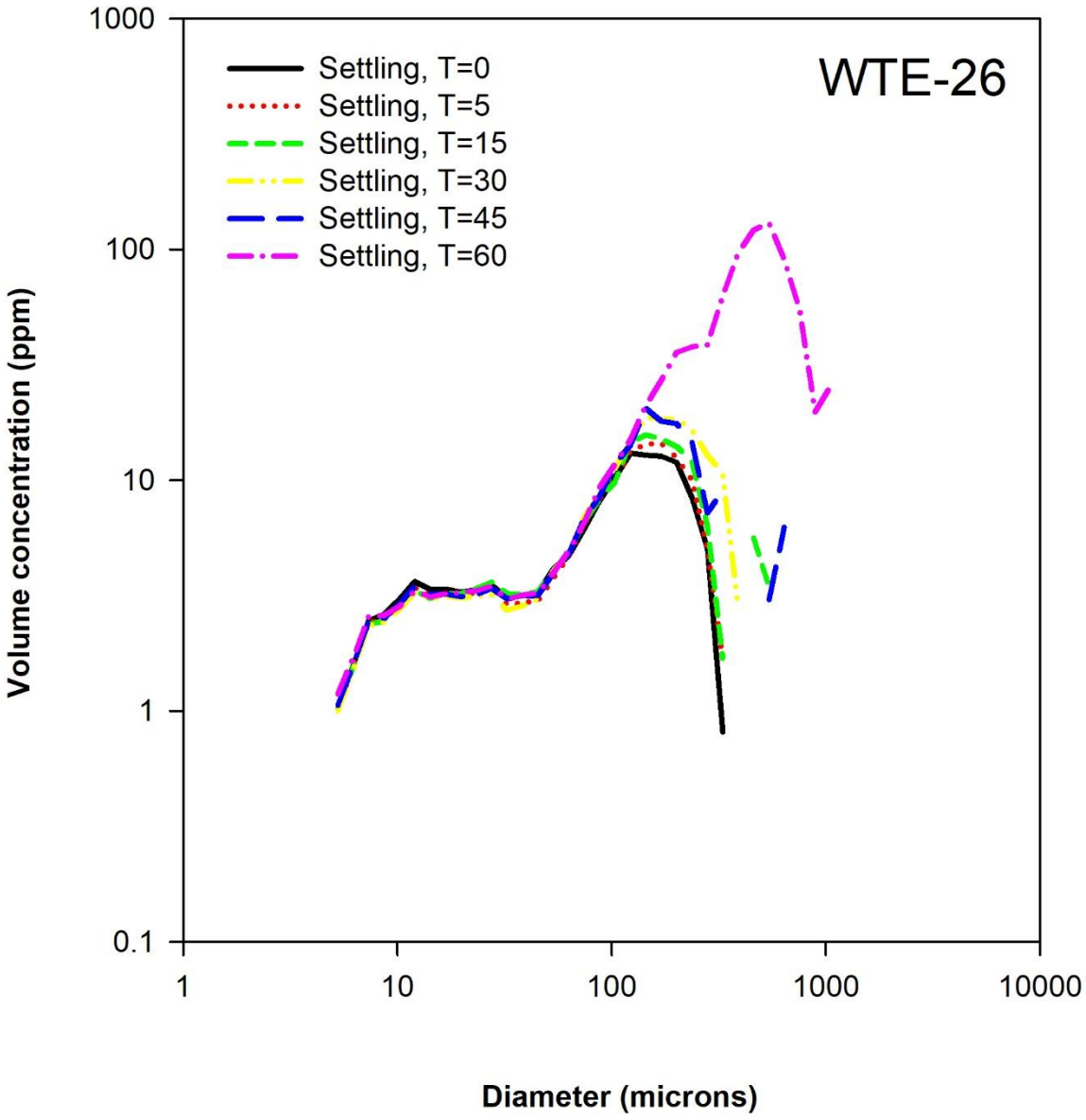

Figure 28: *Merged size spectra from the MVFC & LISST, characterizing the settling phase of WTE-26, at 5 and 15 minute increments. Data are plotted as the log of volume concentration (ppm) versus the log of particle diameter (µm).*

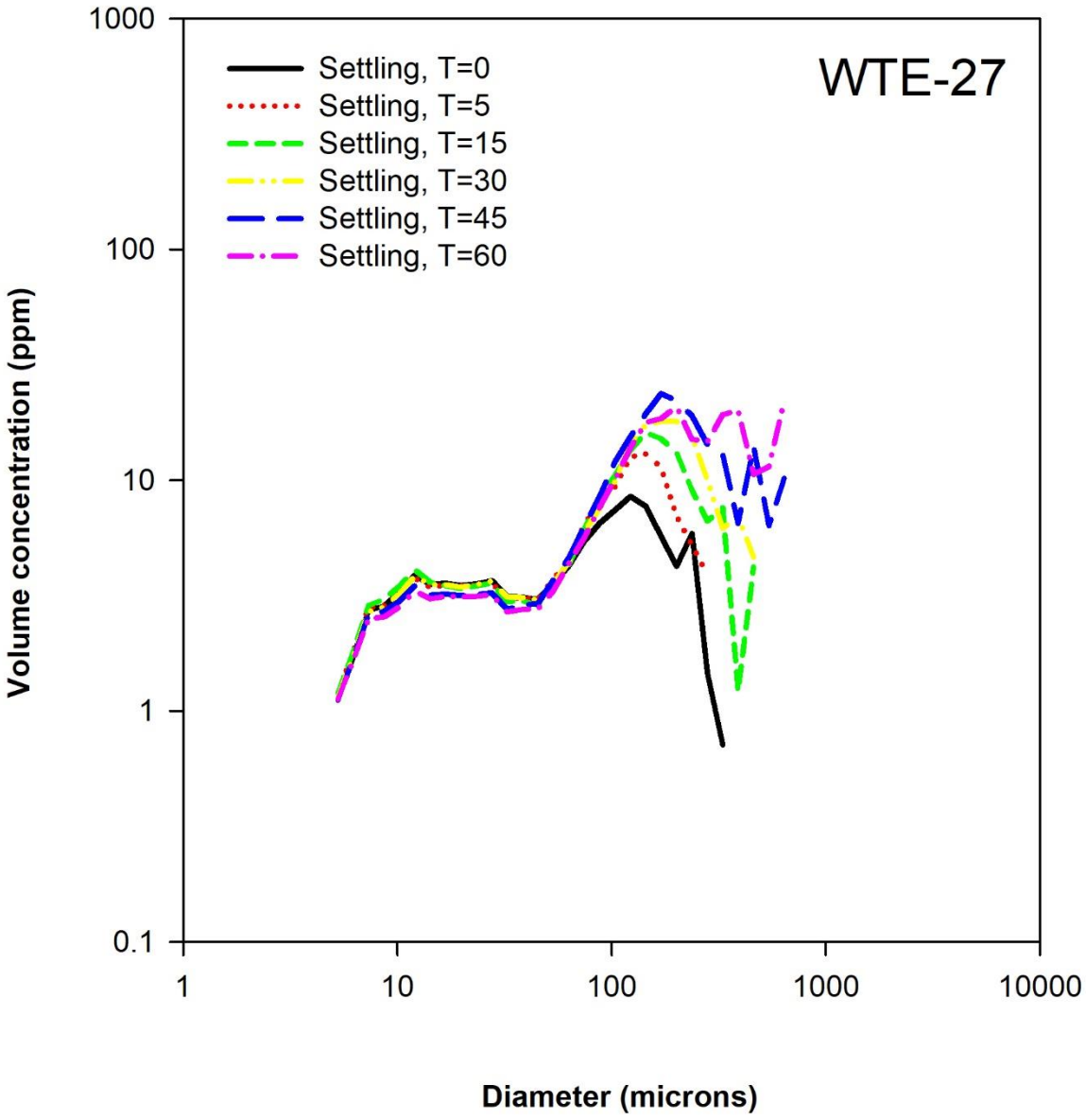

Figure 29: *Merged size spectra from the MVFC & LISST, characterizing the settling phase of WTE-27, at 5 and 15 minute increments. Data are plotted as the log of volume concentration (ppm) versus the log of particle diameter (µm).*

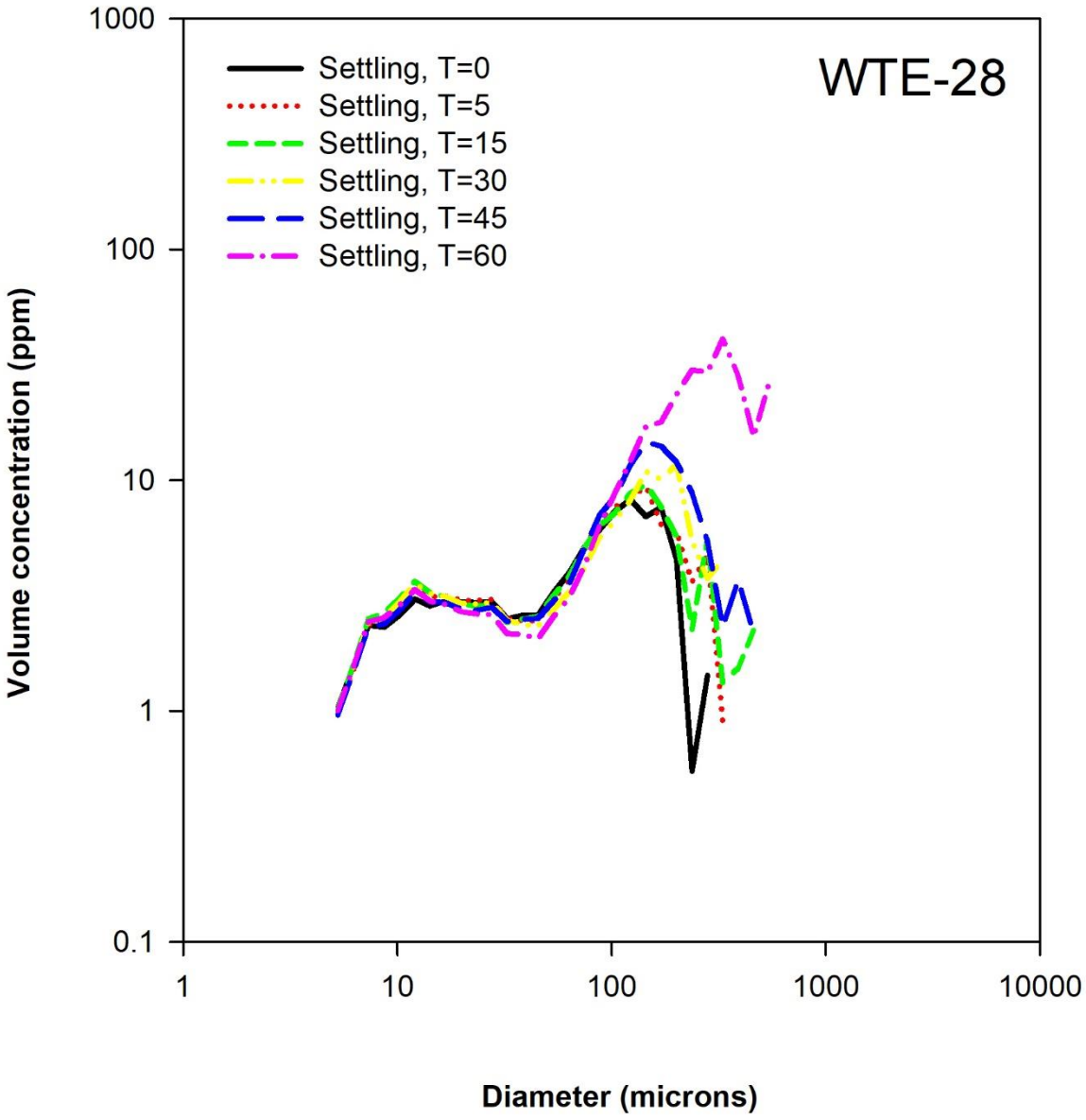

Figure 30: *Merged size spectra from the MVFC & LISST, characterizing the settling phase of WTE-28, at 5 and 15 minute increments. Data are plotted as the log of volume concentration (ppm) versus the log of particle diameter (µm).*

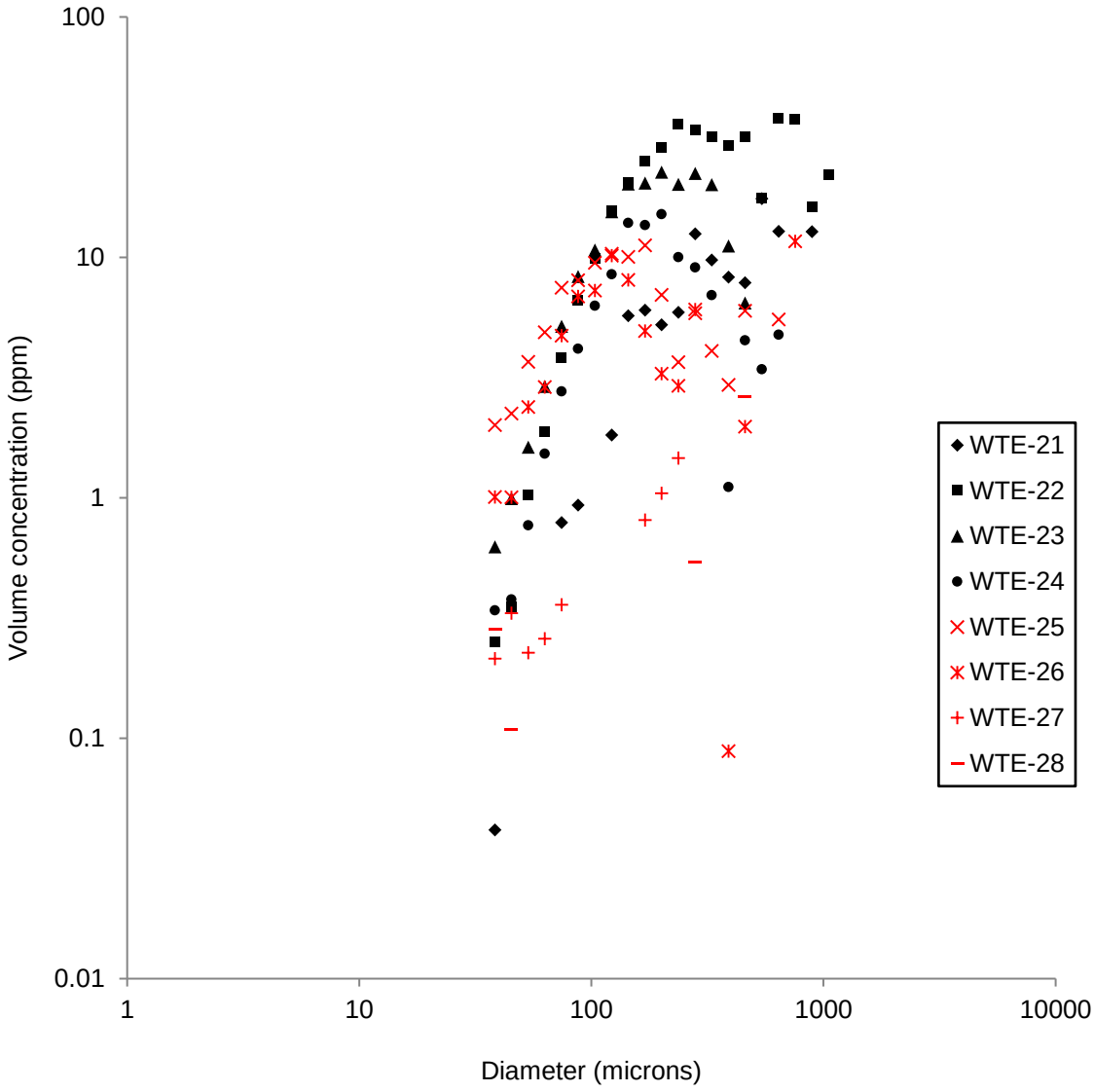

Figure 31: *The size of suspended oil droplets, plotted as the log of volume concentration (ppm) versus that of particle diameter (µm). Oil droplet merged particle size spectra were derived from MVFC imagery captured pre- and post-oil. Colder water (3-8°C) experiments are shown in black, and warmer water (>15°C) in red.*

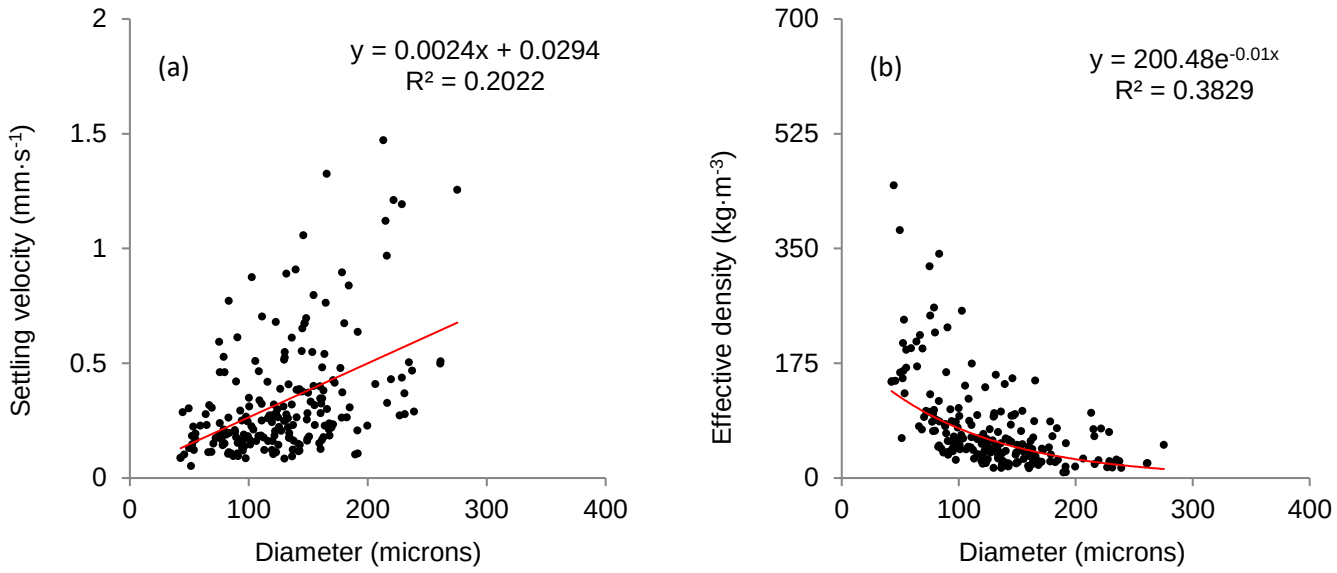

Figure 32: *Plots of particle diameter (µm) versus settling velocity (mm·s^{-1}) and effective particle density (kg·m^{-3}) relationships for WTE-21 in colder water (3.4°C), fitted to linear (a) and power law models (b).*

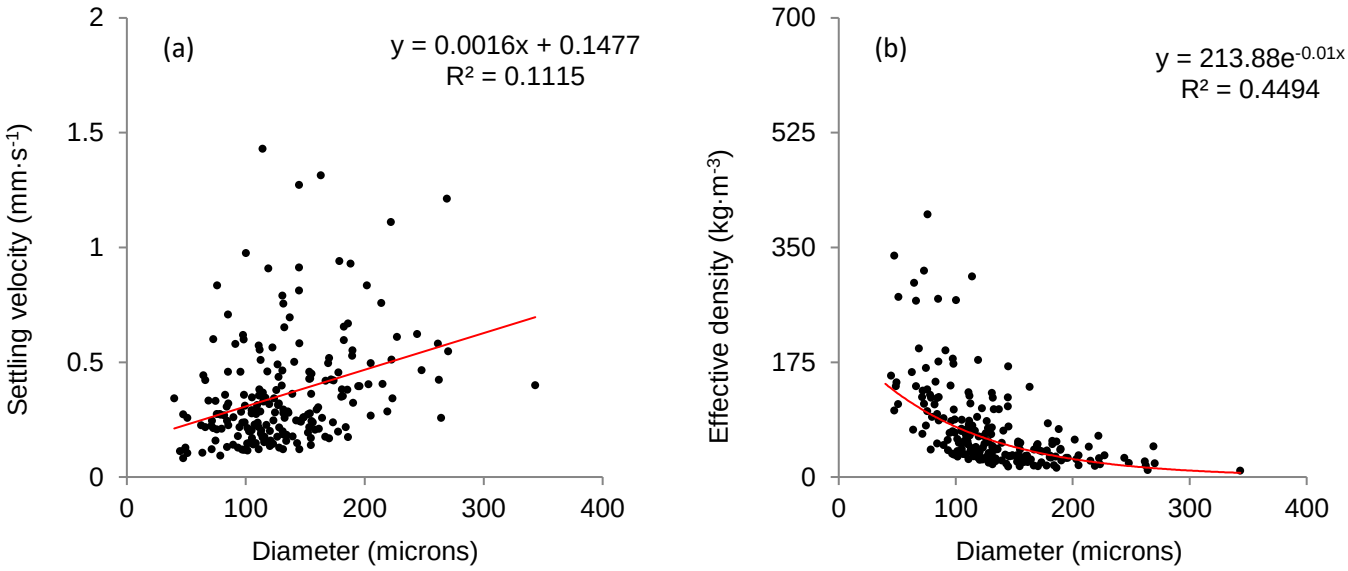

Figure 33: *Plots of particle diameter (µm) versus settling velocity (mm·s^{-1}) and effective particle density (kg·m^{-3}) relationships for WTE-22 in colder water (6.5°C), fitted to linear (a) and power law models (b).*

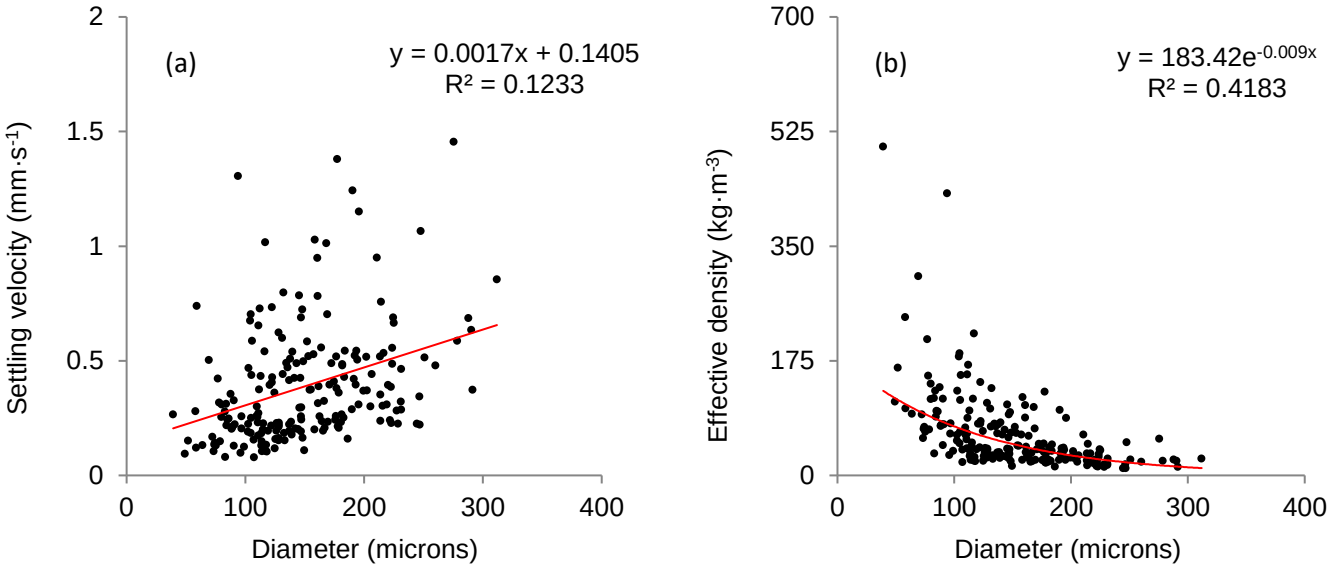

Figure 34: *Plots of particle diameter (µm) versus settling velocity (mm·s^{-1}) and effective particle density (kg·m^{-3}) relationships for WTE-23 in colder water (5.1°C), fitted to linear (a) and power law models (b).*

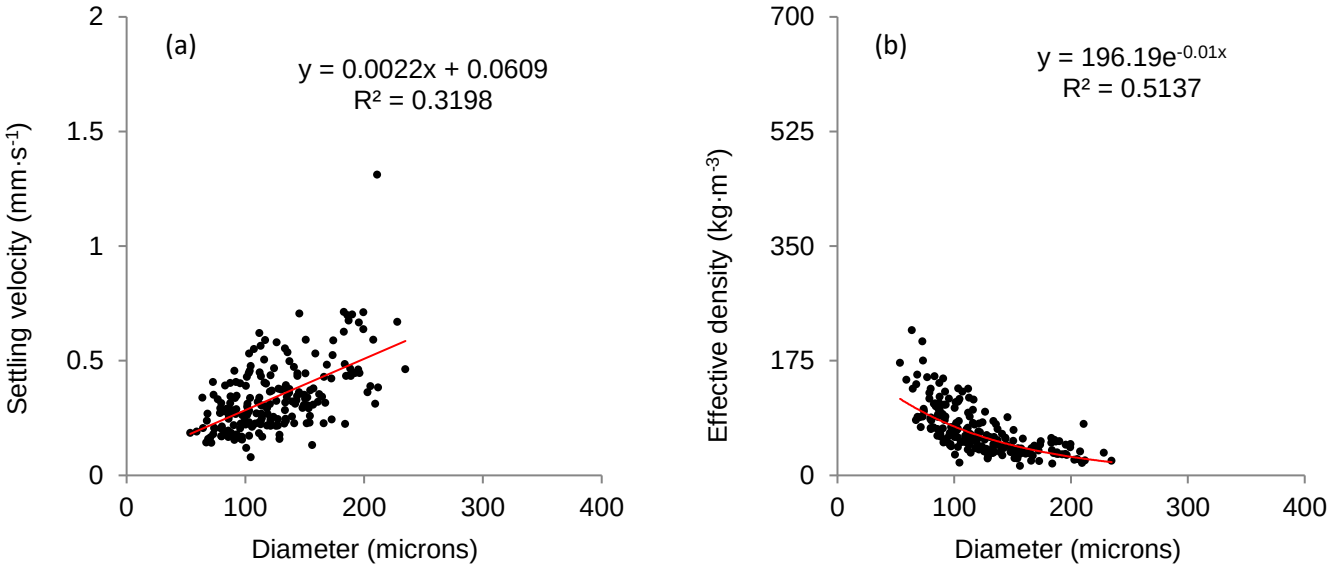

Figure 35: *Plots of particle diameter (µm) versus settling velocity (mm·s^{-1}) and effective particle density (kg·m^{-3}) relationships for WTE-24 in colder water (8.0°C), fitted to linear (a) and power law models (b).*

Table 3: *Results of size settling analysis for four wave tank experiments discussed here. Water temperature (°C) and salinity (ppt) are shown with average particle size (µm), settling velocity (mm·s^{-1}) and effective particle density (kg·m^{-3}).*

Experiment	H2O temp. (°C)	Salinity (ppt)	Avg. Size (µm)	Settling V. (mm·s^{-1})	Effective Density (kg·m^{-3})
WTE-21	3.4	29.5	129.75	0.33	76.65
WTE-22	6.5	27.3	132.12	0.36	75.57
WTE-23	5.1	28.7	149.10	0.39	66.48
WTE-24	8	29.6	123.94	0.34	67.64

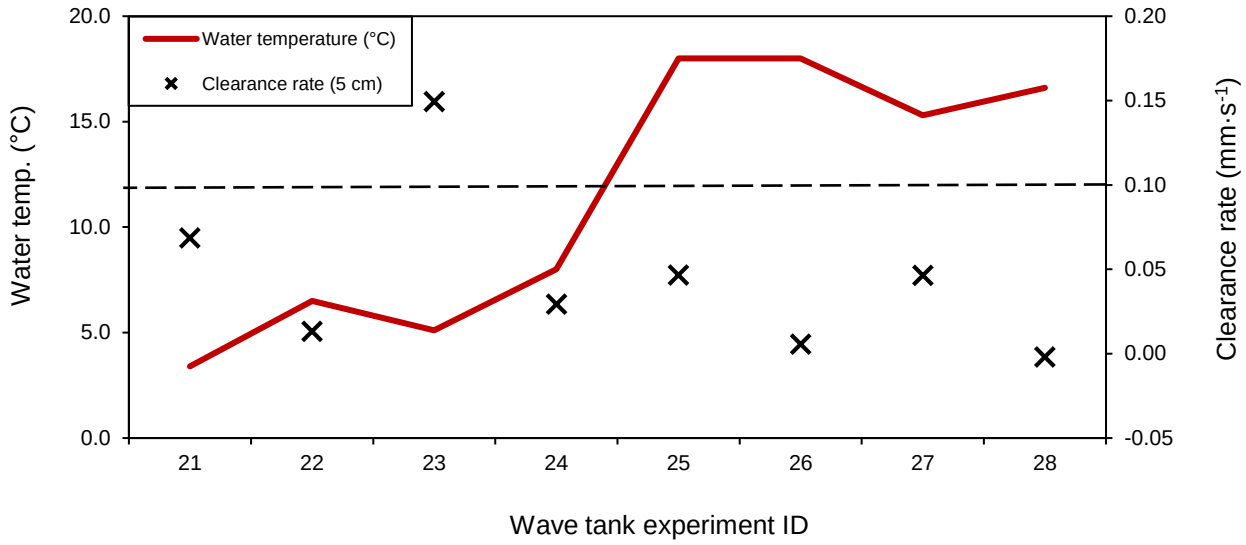

Figure 36: *Plot of water temperature (°C) and clearance rate at 5 cm depth (mm·s^{-1}) for 2014-15 wave tank experiments. The black dashed line (aligned at clearance rate 0.1 mm·s^{-1}) shows general reported clearance rate for high concentrations of fine flocculated marine sediment (Curran et al., 2004, 2002; Hill et al., 2000). Experiment is indicated along the x-axis by wave tank experiment ID; corresponding experimental parameters can found be in Table 5.*

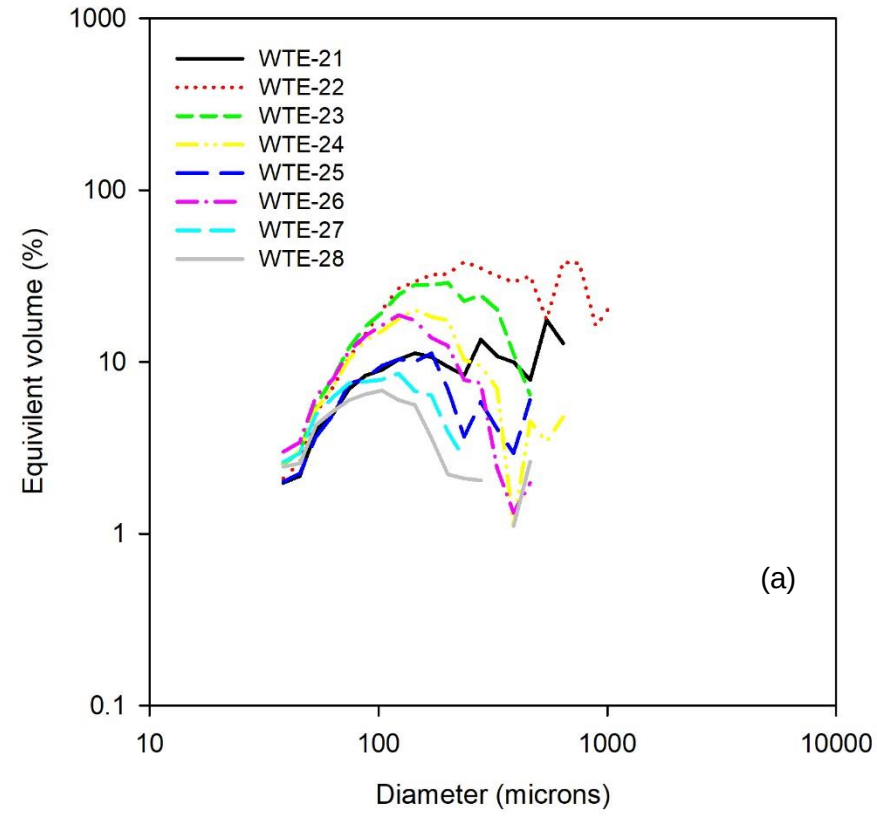

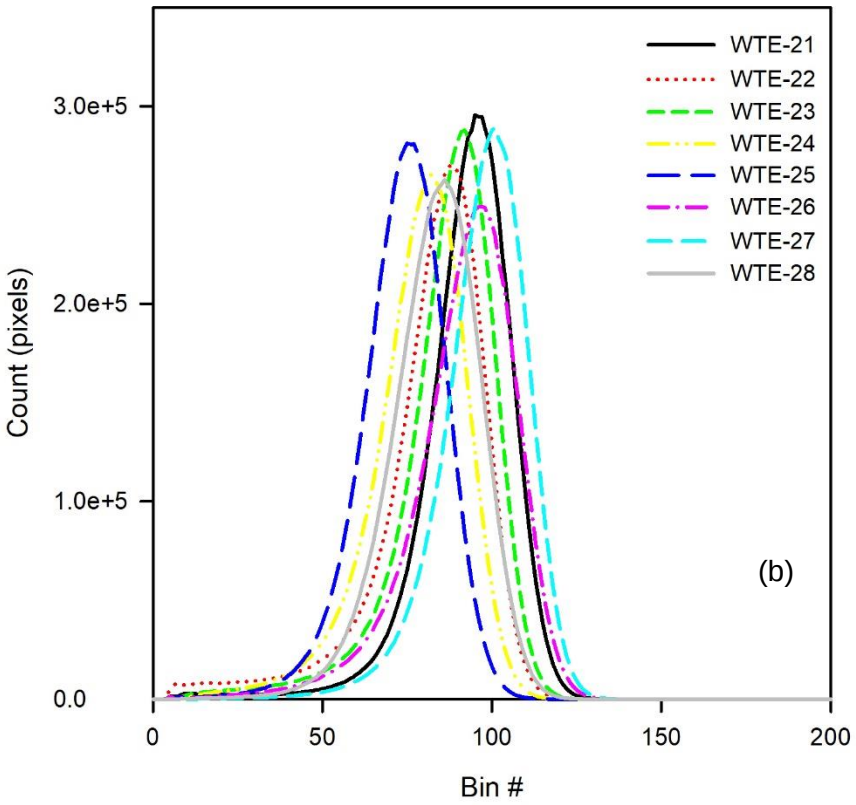

Figure 37: *(a) Particle size spectra derived from MVFC images collected immediately after the addition of dispersed oil are plotted as the log of equivalent volume (%) versus the log of particle diameter (µm); (b) The full greyscale spectra, plotted as bin number (1-255) versus the number of pixels in each, allows a simple comparison of how well particles were dispersed in the wave tank.*

Table 4: *Summary of wave tank experimental parameters (2014-17), showing experimental conditions (S=sediment, O=oil & D=dispersant) and results, including successful OMA production. Dilbits and oils used were Access Western Blend (AWB), Cold Lake Blend (CLB), Western Canadian Select (WCS) and Heidrun.*

Expt.	Expt. conditions	Sediment Conc. (mg/L)	H_2O temp. (°C)	Salinity (ppt)	Oil (type)	D.O.R. (disp:oil)	Settling (duration)	OMA?
WTE2014-3	S, O, D	15.0	4.0	28.5	AWB	1:20	1 hr	No
WTE2014-4	S, O	15.0	6.0	29.7	CLB	1:20	1 hr	No
WTE2014-5	S, O, D	15.0	9.0	30.0	AWB	1:20	1 hr	No
WTE2014-7	S, O	15.0	7.5	30.3	AWB	1:20	1 hr	No
WTE2014-8	S, O	15.0	10.2	29.6	AWB	1:20	1 hr	No
WTE2014-9	S, O, D	15.0	10.2	30.3	CLB	1:20	1 hr	No
WTE2014-10	S, O, D	15.0	9.6	30.4	AWB	1:20	1 hr	No
WTE2014-11	S, O, D	15.0	12.9	30.2	CLB	1:20	1 hr	No
WTE2014-12	S, O	15.0	11.5	29.1	CLB	1:20	1 hr	No
WTE2014-13	S, O, D	15.0	13.1	29.6	CLB	1:20	1 hr	No
WTE2014-15	S, O, D	15.0	13.8	30.2	AWB	1:20	1 hr	No
WTE2014-16	S, O	15.0	14.2	28.1	AWB	1:20	1 hr	No
WTE2014-17	S, O, D	15.0	12.1	30.7	AWB	1:20	1 hr	No
WTE2014-18	S, O	15.0	13.2	31.1	AWB	1:20	1 hr	No
WTE2014-19	S, O, D	15.0	14.0	30.8	AWB	1:20	1 hr	No
WTE2014-20	S, O	15.0	13.2	31.3	AWB	1:20	1 hr	No
WTE2015-21	S, O, D	50.0	3.4	29.5	CLB	1:10	1 hr	No
WTE2015-22	S, O, D	50.0	6.5	27.3	CLB	1:10	1 hr	No
WTE2015-23	S, O, D	50.0	5.1	28.7	AWB	1:10	1 hr	No
WTE2015-24	S, O, D	50.0	8.0	29.6	AWB	1:10	1 hr	No
WTE2015-25	S, O, D	50.0	18.0	29.1	CLB	1:10	1 hr	No
WTE2015-26	S, O, D	50.0	18.0	29.0	CLB	1:10	1 hr	No
WTE2015-27	S, O, D	50.0	15.3	29.2	AWB	1:10	1 hr	No
WTE2015-28	S, O, D	50.0	16.6	28.4	AWB	1:10	1 hr	No
WTE2016-01	S, O, D	50.0	16.8	29.0	AWB	1:10	22 hrs	Yes
WTE2016-02	S, O, D	50.0	17.5	28.4	AWB	1:10	22 hrs	Yes
WTE2016-03	S, O, D	50.0	16.3	28.8	AWB	1:10	22 hrs	Yes
WTE2016-04	S, O, D	50.0	18.2	29.2	AWB	1:10	22 hrs	Yes
WTE2016-05	S, O	50.0	13.9	28.4	AWB	1:10	22 hrs	Yes
WTE2017-01	S, O, D	50.0	16.2	15.3	WCS	1:20	1 hr	Yes
WTE2017-02	S, O, D	50.0	16.5	15	WCS	1:20	1 hr	Yes
WTE2017-03	S, O, D	50.0	16.4	14.7	WCS	1:20	1 hr	Yes
WTE2017-04	S, O, D	50.0	16.1	15.3	Heidrun	1:20	1 hr	Yes
WTE2017-05	S, O, D	50.0	17.3	14.5	Heidrun	1:20	1 hr	Yes
WTE2017-06	S, O, D	50.0	16.2	15.6	Heidrun	1:20	1 hr	Yes

Table 5: *Dispersion efficacy (DE) (%) for wave tank experiments using Douglas Channel sediments with AWB/CLB dilbit treated with/without Corexit 9500A. Note that an efficacy of 100% would indicate that all of the oil added to the tank was dispersed into the water column. Dispersion efficacy at two points during each experiment are shown: T = 120 (end of mixing B) and T = 180 (end of settling).*

Dispersion efficacy (DE) (%)	**WTE-21**	**WTE-22**	**WTE-23**	**WTE-24**	**WTE-25**	**WTE-26**	**WTE-27**	**WTE-28**
% DE at T=120	20.0	28.1	33.1	8.6	65.2	40.6	89.0	60.5
% DE at T=180	13.3	19.2	1.4	0.6	26.5	36.8	71.8	58.9